AMERICAN SOCIETY FOR MICROBIOLOGY | Journal of Virology®

VIRUS-CELL INTERACTIONS

Human Cytomegalovirus Replication Is Inhibited by the Autophagy-Inducing Compounds Trehalose and SMER28 through Distinctively Different Mechanisms

Alex E. Clark,[a,b] Maite Sabalza,[a,b]* Philip L. S. M. Gordts,[c,d] Deborah H. Spector[a,b]

[a]Department of Cellular and Molecular Medicine, University of California—San Diego, La Jolla, California, USA

[b]Skaggs School of Pharmacy and Pharmaceutical Sciences, University of California—San Diego, La Jolla, California, USA

[c]Department of Medicine, Division of Endocrinology and Metabolism, University of California—San Diego, La Jolla, California, USA

[d]Glycobiology Research and Training Center, University of California—San Diego, La Jolla, California, USA

ABSTRACT Human cytomegalovirus (HCMV) is the top viral cause of birth defects worldwide, and current therapies have high toxicity. We previously reported that the mTOR-independent autophagy-inducing disaccharide trehalose inhibits HCMV replication in multiple cell types. Here, we examine the mechanism of inhibition and introduce the autophagy inducer SMER28 as an additional inhibitor of HCMV acting through a different mechanism. We find that trehalose induces vacuolation and acidification of vacuoles and that debris, including debris with an appearance consistent with that of abnormal virions, is present in multivesicular bodies. Trehalose treatment increased the levels of Rab7, a protein required for lysosomal biogenesis and fusion, and slightly decreased the levels of Rab11, which is associated with recycling endosomes. We also present evidence that trehalose can promote autophagy without altering cellular glucose uptake. We show that SMER28 inhibits HCMV at the level of early protein production and interferes with viral genome replication in a cell type-dependent fashion. Finally, we show that SMER28 treatment does not cause the vacuolation, acidification, or redistribution of Rab7 associated with trehalose treatment and shows only a modest and cell type-dependent effect on autophagy. We propose a model in which the reciprocal effects on Rab7 and Rab11 induced by trehalose contribute to the redirection of enveloped virions from the plasma membrane to acidified compartments and subsequent degradation, and SMER28 treatment results in decreased expression levels of early and late proteins, reducing the number of virions produced without the widespread vacuolation characteristic of trehalose treatment.

IMPORTANCE There is a need for less toxic HCMV antiviral drugs, and modulation of autophagy to control viral infection is a new strategy that takes advantage of virus dependence on autophagy inhibition. The present study extends our previous work on trehalose by showing a possible mechanism of action and introduces another autophagy-inducing compound, SMER28, that is effective against HCMV in several cell types. The mechanism by which trehalose induces autophagy is currently unknown, although our data show that trehalose does not inhibit cellular glucose uptake in cells relevant for HCMV replication but instead alters virion degradation by promoting acidic vacuolization. The comparison of our cell types and those used by others highlights the cell type-dependent nature of studying autophagy.

KEYWORDS SMER28, autophagy, cytomegalovirus, trehalose

Received 30 November 2017 **Accepted** 5 December 2017

Accepted manuscript posted online 13 December 2017

Citation Clark AE, Sabalza M, Gordts PLSM, Spector DH. 2018. Human cytomegalovirus replication is inhibited by the autophagy-inducing compounds trehalose and SMER28 through distinctively different mechanisms. J Virol 92:e02015-17. https://doi.org/10.1128/JVI.02015-17.

Editor Rozanne M. Sandri-Goldin, University of California, Irvine

Address correspondence to Deborah H. Spector, dspector@ucsd.edu.

* Present address: Maite Sabalza, Department of Basic Sciences and Craniofacial Development, New York University College of Dentistry, New York, New York, USA.

Human cytomegalovirus (HCMV) is the major viral cause of birth defects and causes severe disease in immunocompromised individuals. It has also been linked with vascular diseases, atherosclerosis, and glioblastoma. Currently, there is no vaccine to prevent infection or transmission to the fetus, and the few drugs available for treatment have associated toxicity. In view of the multiple clinical problems associated with HCMV, there is a need to develop new approaches for preventing infection. Previously, we reported that the disaccharide trehalose, which is a nontoxic mTOR-independent inducer of autophagy, inhibits HCMV infection in multiple human cell types, including human foreskin fibroblasts (HFFs), human aortic artery endothelial cells (HAECs), and cells of the neural lineage derived from human embryonic stem cells (1). Treatment of all of these cells with trehalose induced autophagy and inhibited viral gene expression and the production of extracellular virus. In neural cells, trehalose also reduced the cytopathic effects of the virus that led to limited neurite growth and cytomegaly.

Macroautophagy (here referred to as autophagy) is a degradative pathway that is distinct from ubiquitin-proteasome-mediated degradation. It involves the formation of double-membrane vesicles (autophagosomes) that engulf regions of the cytoplasm (including organelles, protein aggregates, and pathogens) and fuse with the lysosome to form the autolysosome, where the cytoplasmic cargo is degraded and nutrients are recycled. Autophagosomes can also fuse with early endosomes or late endosomes/multivesicular bodies (MVBs) to form amphisomes, which then fuse with the lysosome. Amphisomes may also contain small amounts of the lysosomal V-type ATPase, which would facilitate their acidification (2). Multiple Atg (autophagy-related) proteins are associated with the autophagy pathway, and complexity is further increased by recent data showing the interplay of the endocytic and autophagy molecular machinery (3). Rab7 is a notable example of a small GTPase with pleiotropic functions in vesicle trafficking (for a recent review, see reference 4). It plays a role in the maturation of early endosomes to late endosomes, whereby Rab5 associated with early endosomes is replaced by Rab7. Rab7 is also involved in the biogenesis of lysosomes, transport from late endosomes to lysosomes, the fusion of late endosomes with lysosomes, and the final maturation of autophagic vesicles to autolysosomes.

There is increasing evidence that herpesviruses make use of the autophagy pathway for secondary envelopment and egress from cells. The details of the assembly of herpesvirus infectious particles are not fully clear. However, the consensus is that capsids loaded with the DNA genome are enveloped as they bud through the inner nuclear envelope (primary envelopment) and are deenveloped as they pass across the outer nuclear membrane into the cytosol. Generally, the capsid then acquires tegument proteins by budding into vesicles coated with viral tegument proteins and glycoproteins and acquires its final envelope (secondary envelopment) in the cytoplasm. There is extensive remodeling of cellular membranes, but the mechanisms of secondary envelopment and egress and the source of the membranes remain unclear and likely depend on the specific herpesvirus and cell type (for a review, see reference 5). Recent studies, however, indicate that some herpesviruses, including Epstein-Barr virus (EBV), Kaposi's sarcoma-associated herpesvirus (KSHV), and varicella-zoster virus (VZV), may use autophagic membranes for this secondary envelopment (6–9). In the case of EBV and KSHV, autophagy is blocked prior to the fusion of the autophagosome and lysosome, and this is associated with a specific reduction in Rab7 levels (7, 8).

In cells infected with either HCMV or the related betaherpesvirus human herpesvirus 6A (HHV-6A), there is extensive reorganization of cellular membranes into seemingly concentric layers around the microtubule-organizing center (MTOC) to form the perinuclear cytoplasmic assembly compartment. This compartment is comprised of protein markers normally present in early endosomes, *trans*-Golgi network (TGN), Golgi, and endoplasmic reticulum (ER) membranes, but excludes the lysosomal markers Lamp1 and Lamp2 (10–13). Notably, TGN46; the endosomal markers annexin 1, early endosomal antigen 1 (EEA1), and transferrin receptor; the cation-independent mannose 6-phopshate receptor (which traffics between the TGN and the endosome); and CD63 (the late endosome/multivesicular body [MVB] and exosome marker) are all associated

with secondary envelopment and egress, suggesting that recycling endosomes and the exosomal release pathway are involved (12, 14, 15). It has been shown that the cytoplasmic envelopment of HCMV may be initiated by a tubular crescent-shaped membrane that wraps around the capsid (16, 17). Fusion of the edges of the membrane results in an enveloped viral particle within the vesicle. Budding of viral capsids into MVBs has also been observed. These vesicles traffic to the plasma membrane, where they release the mature enveloped virus by exocytosis. However, the precise composition and identity of these vesicles have yet to be elucidated. Electron microscopy (EM) studies have also demonstrated that T cells infected with HHV-6A have an increased number of MVBs that contain viral particles (14). MVB fusion at the plasma membrane and small vesicles and viral particles at the cell surface were also observed, suggesting the targeting of the MVBs to the cell surface. It is known that late endosomes/MVBs, which contain intraluminal vesicles (ILVs) ranging in size from 30 to 100 nm, can be targeted to either the lysosome for degradation of the MVB contents or the plasma membrane for release of the MVB contents extracellularly.

In our previous work, we noted that treatment of HFFs and HAECs with trehalose dramatically decreased the amount of extracellular virus produced while having only a modest inhibitory effect on cell-associated virus (1). This suggested that the induction of autophagy by trehalose may have affected viral trafficking by preventing the transport of mature virions to the plasma membrane for release into the extracellular environment. In the studies reported here, we examine the mechanism underlying the inhibition of HCMV infection in HFFs and HAECs by trehalose. We show that contrary to previous reports stating that trehalose functions through the reduction of glucose uptake into hepatocytes (18, 19), there is no restriction of glucose uptake during trehalose treatment in uninfected or HCMV-infected HFFs and HAECs. By electron microscopy, we show that trehalose treatment results in extensive vacuolation and altered morphology of MVBs. The vesicles are acidified, and MVBs contain more debris and virus particles with apparent abnormalities such as asymmetry and wrinkling of the envelope. Consistent with an alteration in trafficking and extracellular release of mature virions, there is also a reciprocal effect on the levels of two Rabs, with an increase in the level of Rab7 and a decrease in the level of Rab11. These Rabs are important for autophagosome-lysosome fusion and the transport of vesicles to the plasma membrane, respectively.

Additionally, we compare the effect of trehalose on HCMV infection with that of another mTOR-independent autophagy inducer, SMER28. SMER28 was initially discovered in a screen for enhancers of the cytotoxic effects of rapamycin in yeast (20). Treatment of HeLa cells stably expressing transfected enhanced green fluorescent protein (EGFP)-LC3 with SMER28 resulted in increased numbers of LC3B-positive puncta and increased levels of EGFP–LC3B-II, suggesting increased autophagosome levels (20). Further testing showed that it was mTOR independent and was able to induce the clearance of autophagy substrates, including mutant huntingtin associated with Huntington's disease, A53T α-synuclein in a Parkinson's disease model, and Aβ peptide and the amyloid precursor protein-derived C-terminal fragment (APP-CTF) in an Alzheimer's disease model (20, 21). Aggregate clearance was reported to be ATG5 dependent based on data from ATG5$^{-/-}$ mouse embryonic fibroblasts (MEFs). In addition, SMER28 inhibited the replication of Rift Valley fever virus in mammalian cells, reinforcing the possibility of autophagy regulation as a therapeutic option (22). Recently, SMER28 has gained attention for its ability to enhance the differentiation of MEFs along a neural lineage and to stimulate the erythropoiesis of K562 bone marrow cells *in vitro* and *in vivo*, both of which were dependent on the presence of ATG5 (23, 24). We find that in HCMV-infected HFFs and HAECs treated with SMER28, there is a significant inhibition of both cell-associated and cell-free virus production, with a greater effect on released virus. The mechanism appears to differ from that of trehalose, as there is a major reduction in the expression levels of both early and late genes, and there is no induction of extensive vacuolation or acidification of vesicles. There is also inhibition of viral DNA synthesis in HAECs but not in HFFs.

RESULTS

Trehalose treatment of infected and uninfected cells results in cytoplasmic vacuolation and altered morphology of MVBs. As a follow-up to our studies showing that the disaccharide trehalose inhibits HCMV (referred to by clinical strain name TB40E) in various types of host cells (1), we proceeded to further characterize the molecular mechanisms responsible for this inhibition. Our previous work showed that trehalose treatment reduced cell-free virus production to a greater degree than it reduced cell-associated virus production (1). To visualize the late stages of virus maturation and release, we performed electron microscopy on HFFs infected with TB40E at a multiplicity of infection (MOI) of 1 in the presence or absence of 100 mM trehalose. At 96 hpi, cells were fixed with 2% glutaraldehyde and processed for electron microscopy. In infected samples, only cells with capsids present in the nucleus were imaged at a higher magnification. We observed increased numbers of cytoplasmic vacuoles in the majority of cells in the presence of trehalose, especially in infected cells (Fig. 1D). In addition, MVBs contained more debris, and membrane whorls were present. Although we observed single vesicles with intact virus, indicating that secondary envelopment was not totally impaired (Fig. 1J), there were many MVBs with debris consistent in size and appearance with virions possessing abnormal morphologies, such as a disrupted envelope (Fig. 1K and 2). Trehalose treatment did not disrupt the formation of capsids or the loading of viral DNA into capsids in the nucleus, as there were A, B, and C capsids present with and without trehalose (Fig. 1H and L). Cytoplasmic vacuolation was also observed in uninfected cells treated for 96 h with trehalose and processed for electron microscopy as described above (Fig. 1B). Examples of cytoplasmic vacuoles in additional trehalose-treated cells are shown in Fig. 2.

We also examined the effect of trehalose on HAECs. At 1 day postplating, HAECs were mock infected or infected at an MOI of 3 (to allow infection of the majority of the cells) in the presence or absence of 100 mM trehalose and processed for electron microscopy at 96 h postinfection (hpi). Trehalose treatment resulted in the extensive vacuolation of cells (Fig. 3B and D) and an altered content of MVBs (Fig. 3J and K), similar to what was observed in uninfected and infected HFFs. Similar to HFFs, infected HAEC nuclei contained A, B, and C capsids (Fig. 3H and L). Examples of cytoplasmic vacuoles in additional trehalose-treated HAECs at 96 hpi are shown in Fig. 4. At 120 hpi, there was more extensive cytoplasmic vacuolation and abnormal MVBs in both HFFs (data not shown) and HAECs (Fig. 5) treated with trehalose, and few extracellular virions were observed.

Trehalose does not interfere with cellular glucose uptake in HFFs or HAECs. It was recently reported that trehalose treatment reduces glucose uptake in various cell types, including 293 cells with short hairpin RNA (shRNA) to GLUT1 and overexpressing GLUT1 to -4 or GLUT8, primary murine hepatocytes, and HepG2 human hepatocellular carcinoma cells (18). Since it has been demonstrated that HCMV-infected cells show an increase in glucose uptake (25) and that blocking GLUT4-mediated glucose transport during infection leads to reduced virus production (26), we tested whether the trehalose effect was due to limiting glucose uptake during HCMV infection. We measured the uptake of radiolabeled 2-deoxy-glucose (2DG) by infected and uninfected HFFs and HAECs in the absence or presence of 100 mM trehalose. HFFs or HAECs were infected at a high MOI (MOI of 3) with TB40E or mock infected. At 48 hpi, a glucose uptake assay was performed by using a 15-min incubation with 100 mM trehalose and a total 2DG concentration of 6.5 mM. Cytochalasin B, which inhibits GLUT-mediated glucose uptake, and insulin, which stimulates glucose uptake, were included as controls. Triplicate wells were assayed in each experiment. Neither infected or uninfected HFFs (Fig. 6A) nor HAECs (Fig. 6B) showed reduced glucose uptake in the presence of trehalose. We noted that in HFFs, there was an expected increase in glucose uptake during HCMV infection, and cytochalasin B and insulin induced the expected decrease and increase, respectively. Unexpectedly, both uninfected and infected HAECs showed a small increase in glucose uptake in the presence of trehalose. This increase reached significance

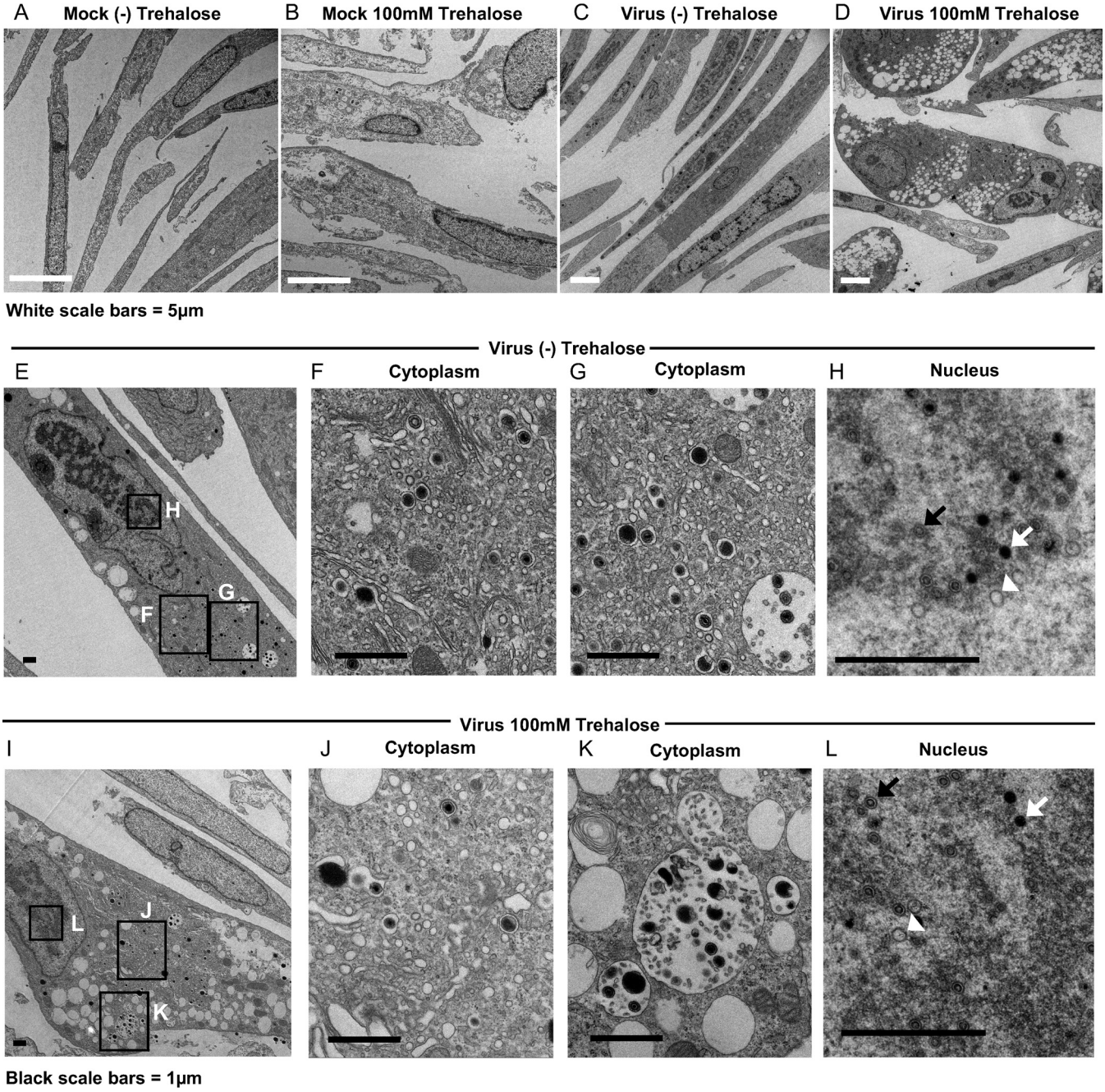

FIG 1 Trehalose induces cytoplasmic vacuolization and alters MVB contents and intra-MVB virion morphology in HFFs. At the time of replating, HFFs were mock infected (A and B) or infected with TB40E at an MOI of 1 (C to L) in the presence or absence of 100 mM trehalose. At 96 hpi, cells were fixed and processed for electron microscopy. Boxes in the left images indicate regions of enlargement in the right images. A, B, and C capsids in panels H and L are indicated by white arrowheads, black arrows, and white arrows, respectively.

only in infected HAECs, likely due to a smaller variation of the conditions in those samples.

Since, in contrast to the studies of DeBosch et al. (18), we did not observe any reduction in glucose uptake, we felt that it was important to repeat the assay under the exact conditions used in the previous study (Fig. 7A [our conditions] and B [conditions of the studies by DeBosch et al.]). A major difference was the concentration of unlabeled 2DG in our assays. We used a concentration of 6.5 mM unlabeled 2DG, which is physiologically relevant, as it is the glucose concentration found in the fasted state in humans and in standard culture media. This concentration is 100-fold higher than

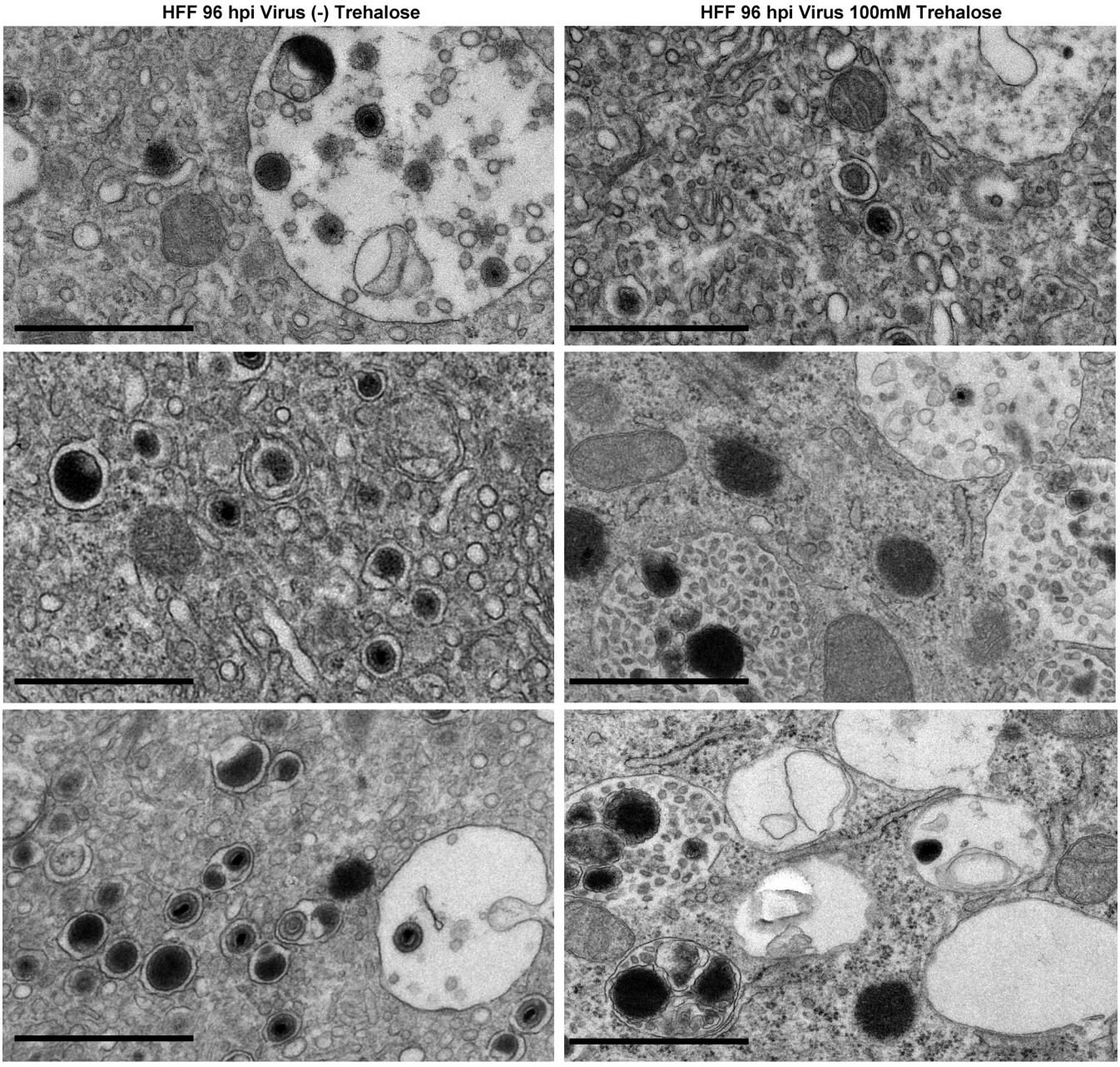

FIG 2 Trehalose treatment of infected HFFs induces vacuoles containing debris and whorls. At the time of replating, HFFs were infected with TB40E at an MOI of 1 in the presence or absence of 100 mM trehalose. At 96 hpi, cells were fixed and processed for electron microscopy. Black bars, 1 μm.

that used by DeBosch et al. (50 μM) to observe a maximal inhibition of glucose uptake by 100 mM trehalose. There was also a difference in the preincubation times in the presence of trehalose in glucose-free buffer (30 min by DeBosch et al. versus 15 min in our assay) and in the times of measuring 2DG uptake (6 min by DeBosch et al. and 5 min in our assay). Additionally, we had incubated the cells for 4 to 6 h in serum-free medium in order to examine the effect of insulin, and this step was eliminated when the two types of conditions were tested in parallel. We performed the experiment with uninfected HFFs using 3 different concentrations of 2DG (50 μM, 500 μM, and 6.5 mM) in the presence or absence of 100 mM trehalose (Fig. 7). We did not observe an inhibition of glucose uptake when cells were treated with trehalose. In fact, at the lower 2DG concentrations, we observed an increase in glucose uptake in the presence of trehalose. As expected, the uptake of radiolabeled 2DG (a fixed amount was used

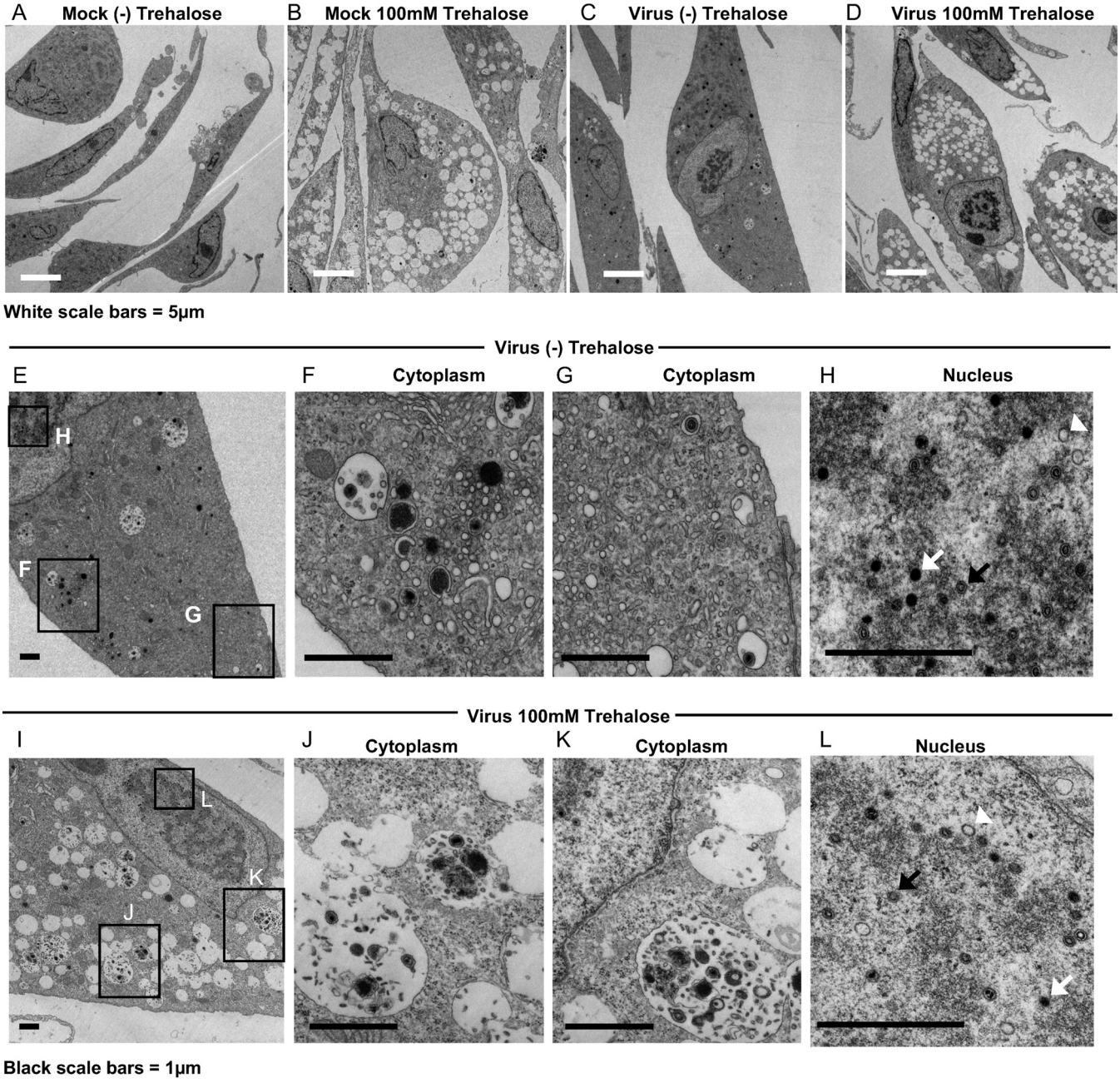

FIG 3 Trehalose induces cytoplasmic vacuolization and alters MVB contents and intra-MVB virion morphology in HAECs. One day after replating, HAECs were mock infected (A and B) or infected with TB40E at an MOI of 3 (C to L) in the presence or absence of 100 mM trehalose. At 96 hpi, cells were fixed and processed for electron microscopy. Boxes in the left images indicate regions of enlargement in the right images. A, B, and C capsids in panels H and L are indicated by white arrowheads, black arrows, and white arrows, respectively.

[0.5 μCi/well]) was greater in the presence of decreasing overall 2-deoxy-glucose concentrations. Taken together, these data show that in primary HFFs and HAECs, which are the *in vivo* targets of HCMV, trehalose did not inhibit glucose uptake.

SMER28 delays progression of HCMV infection. To complement the studies on the mechanisms of trehalose-mediated inhibition of HCMV infection, we evaluated SMER28, another mTOR-independent autophagy inducer, for antiviral activity. We first tested whether SMER28 affects the production of infectious virus by monitoring viral titers at various times postinfection (p.i.) with increasing concentrations of SMER28. HFFs were infected at an MOI of 0.5 in the presence of 25 or 50 μM SMER28 or an equivalent volume of dimethyl sulfoxide (DMSO). The concentration of DMSO did not

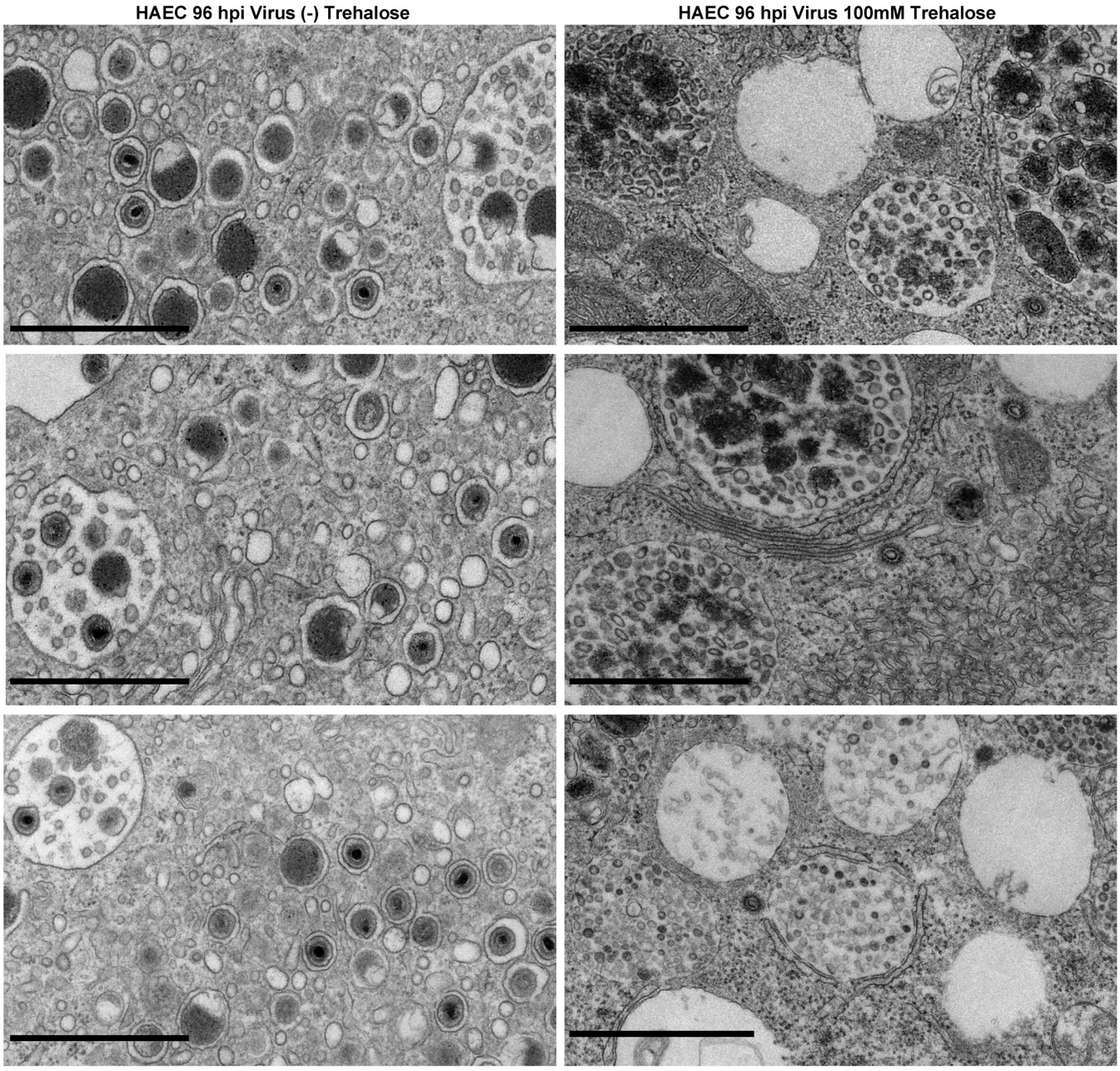

FIG 4 Trehalose induces cytoplasmic vacuolization and alters MVB contents and intra-MVB virion morphology in HAECs at 96 hpi. One day after replating, HAECs were infected with TB40E at an MOI of 3 in the presence or absence of 100 mM trehalose. At 96 hpi, cells were fixed and processed for electron microscopy. Black bars,1 μm.

exceed 0.05% by volume in the culture media, and at these concentrations of SMER28, there was no toxic effect on the cells. In the case of HAECs, the cells were infected at an MOI of 3 and treated with DMSO or 50 μM SMER28. At 24, 72, and 120 hpi, cell pellets and supernatants were collected. Plaque assays showed that similar to the effect of trehalose, there was a reduction in the amount of cell-free virus in both HFFs (Fig. 8A, left) and HAECs (Fig. 8B, left). Furthermore, in contrast to trehalose, SMER28 treatment caused a reduction in the amount of cell-associated virus in HFFs (Fig. 8A, right) and HAECs (Fig. 8B, right). Infected HFFs treated with 50 μM SMER28 showed maximum reduction in cell-free and cell-associated viral titers at 72 hpi. For HAECs, the maximal reduction in titers was found at 72 hpi for cell-associated virus and at 120 hpi for cell-free virus.

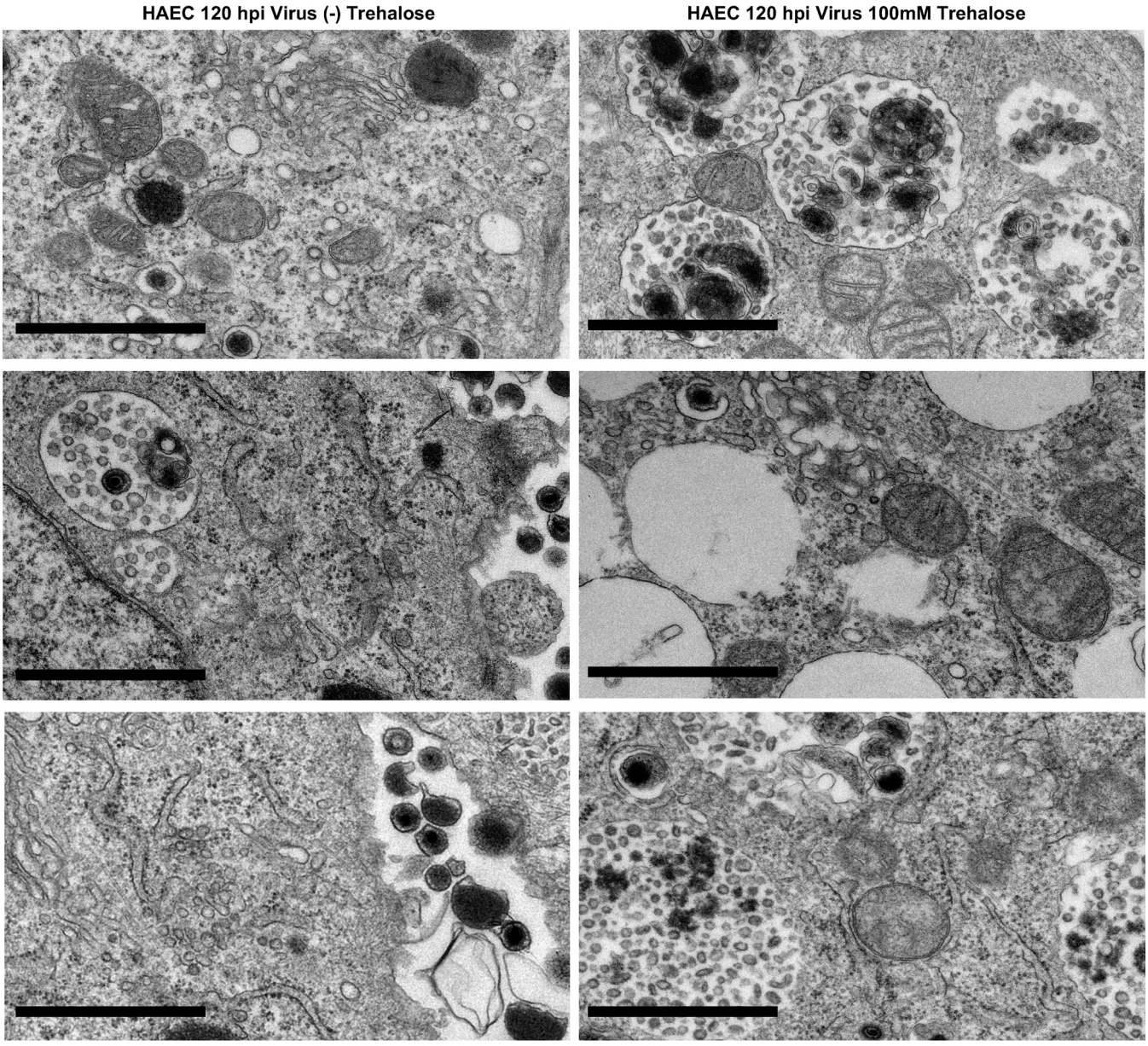

FIG 5 Trehalose induces cytoplasmic vacuolization and alters MVB contents and intra-MVB virion morphology in HAECs at 120 hpi. One day after replating, HAECs were infected with TB40E at an MOI of 3 in the presence or absence of 100 mM trehalose. At 120 hpi, cells were fixed and processed for electron microscopy. Black bars, 1 μm.

To assess where in the infectious cycle SMER28 acted, HFFs (Fig. 9A) and HAECs (Fig. 9B) were infected at an MOI of 0.5 in the presence of 0, 25, or 50 μM SMER28. At the indicated hpi, cell pellets were harvested, and lysates were prepared for Western blot analysis. Western blot analysis showed that SMER28 treatment had some inhibitory effect on the accumulation of the immediate early protein IE1 72 in HFFs and on IE2 86 in both HFFs and HAECs. In addition, there was a dose-dependent decrease in the levels of the early proteins UL44 and UL57 and the late proteins pp28, IE2 40, and IE2 60, with greater inhibition occurring in HAECs. This enhanced reduction in protein levels in HAECs was most notable for the late proteins. We determined that the addition of SMER28 to infected HFFs can be delayed 24 h without a substantial loss of inhibition of viral titers or a reduction in the levels of the viral early and late proteins described above (data not shown), suggesting that the drug acts after the initiation of early gene expression.

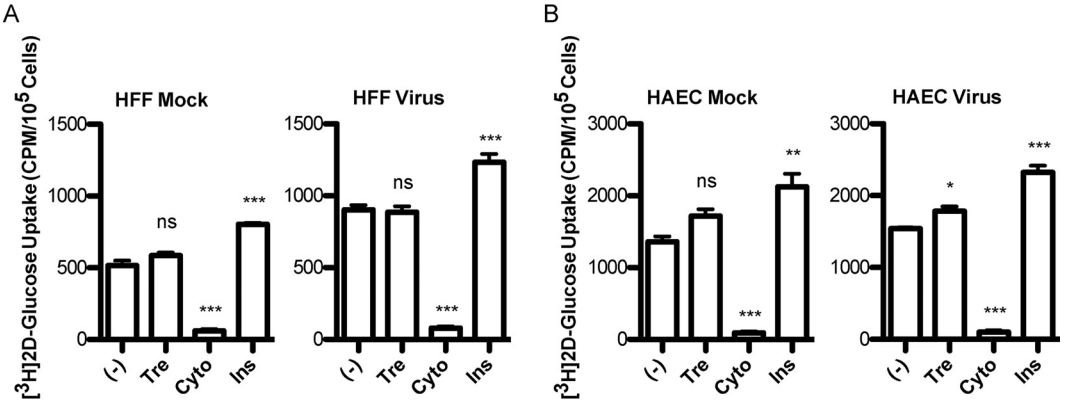

FIG 6 Trehalose does not interfere with cellular glucose uptake. HFFs (A) or HAECs (B) were mock infected or infected with TB40E at an MOI of 3. At 48 hpi, cells under serum-free conditions were untreated (−) or incubated with 100 mM trehalose (Tre), 20 μM cytochalasin B (Cyto), or 200 nM insulin (Ins) for 15 min prior to the addition of radiolabeled [1,2-^{3}H]2-deoxy-D-glucose. The level of radioactivity in cells was assayed by scintillation counting of lysates. In each experiment, the assay was performed on triplicate wells. Error bars indicate standard errors of the means of results from triplicate wells. Significance was determined by one-way ANOVA followed by Dunnett's test. ns, not significant ($P > 0.05$); *, $P \leq 0.05$; **, $P \leq 0.01$; ***, $P \leq 0.001$.

SMER28 inhibits HCMV DNA replication in HAECs but not in HFFs. When the results with SMER28 were compared with those of our previous studies with trehalose, we noted that while both compounds reduce the levels of viral early and late proteins in HFFs and HAECs, SMER28 appeared to have a much greater effect on the late proteins in HAECs. To determine whether trehalose or SMER28 also affected viral DNA replication, HFFs and HAECs were infected at an MOI of 0.5 in the absence or presence of 100 mM trehalose or 50 μM SMER28 and harvested at various times p.i. DNA was extracted from cells, and viral genome copy numbers were measured by quantitative PCR (qPCR) and normalized to the values for cellular glyceraldehyde-3-phosphate dehydrogenase (GAPDH). Fold changes relative to values for untreated samples at 24 hpi are displayed in Fig. 10. There was no inhibition of viral DNA replication in HFFs or HAECs treated with 100 mM trehalose (Fig. 10A and C). This result was not surprising, considering the lack of change in nuclear capsids in Fig. 1 and 3. Interestingly, SMER28 reduced viral DNA replication in HAECs but not in HFFs (Fig. 10B and D). The difference

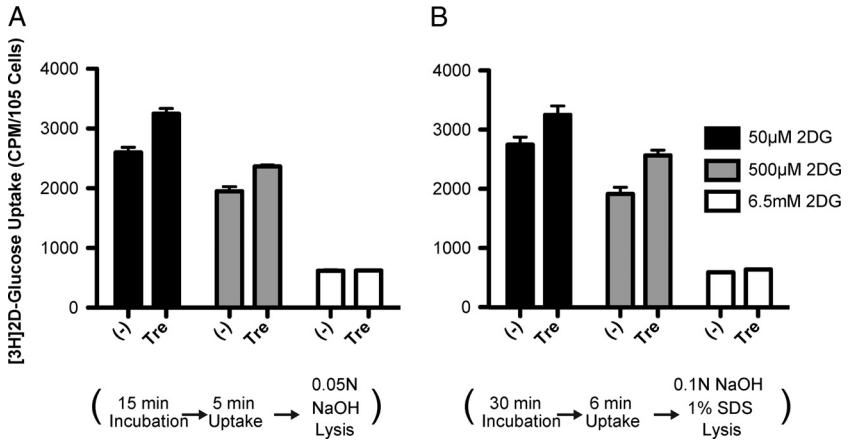

FIG 7 Trehalose does not interfere with cellular glucose uptake under various glucose uptake assay conditions. We compared our assay conditions for glucose uptake (A) with those used by DeBosch et al. (B). Non-serum-starved HFFs were untreated (−) or incubated with 100 mM trehalose (Tre) 15 min (A) or 30 min (B) prior to the addition of radiolabeled [1,2-^{3}H]2-deoxy-D-glucose at the indicated levels of total 2DG. Uptake was allowed for 5 min (A) or 6 min (B) before stopping with ice-cold washes. Lysis was completed by incubation with the indicated solutions. The level of radioactivity in cells was assayed by scintillation counting of lysates. In each experiment, the assay was performed on triplicate wells. Error bars indicate standard errors of the means for triplicate wells.

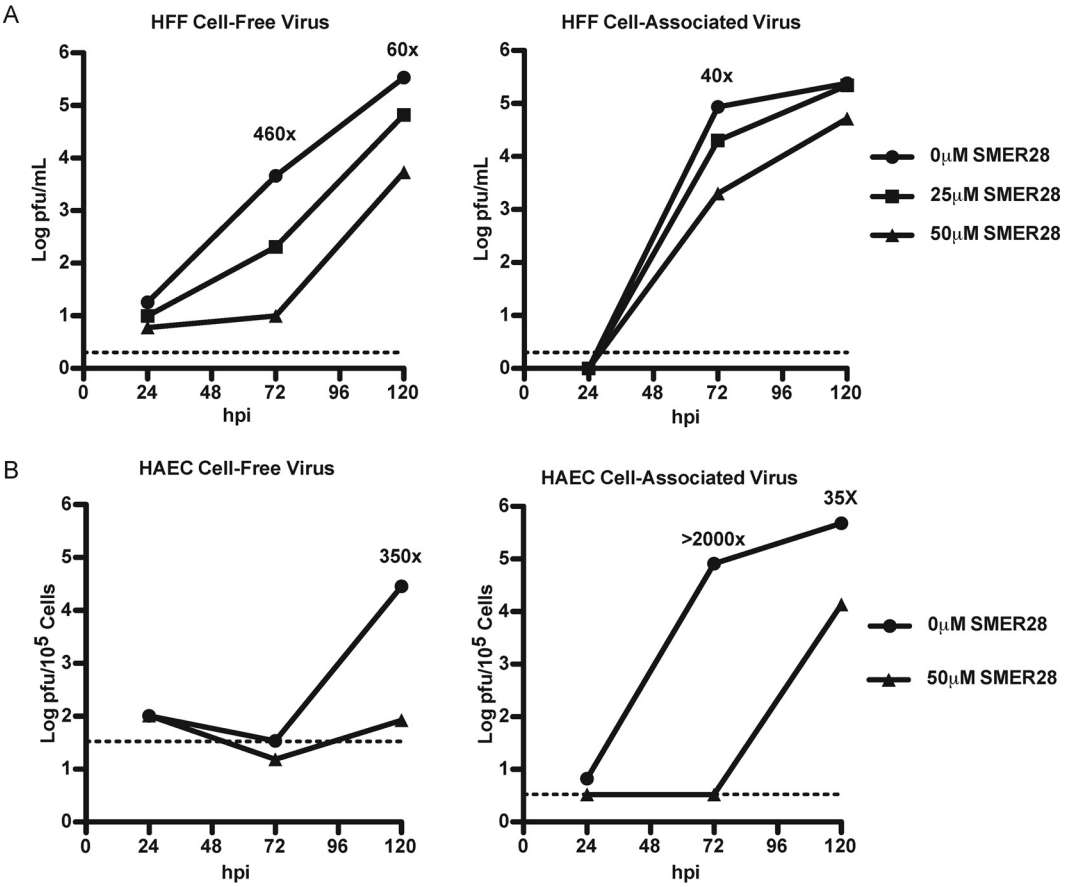

FIG 8 SMER28 delays progression of HCMV infection. HFFs were infected with TB40E at an MOI of 0.5 at the time of replating (A), and HAECs were infected with TB40E at an MOI of 3 1 day after replating (B). A total of 25 or 50 μM SMER28 or DMSO (0) for HFFs or 50 μM SMER28 or DMSO (0) for HAECs was added to the medium at the time of infection. Cell supernatants (left) and cell pellets (right) were harvested at 24, 72, and 120 hpi. Infectious virions were measured by a plaque assay. Fold changes indicate differences between treatments with 50 μM SMER28 and DMSO at the time points shown. The dashed line indicates the limit of detection of each plaque assay.

in viral DNA replication between these cell types is consistent with the greater reduction in late protein levels seen in SMER28-treated HAECs than in HFFs.

SMER28 reduces numbers of enveloped virions in infected cells and does not induce vacuolation of the cytoplasm. We performed electron microscopy on infected cells treated with SMER28 to visualize virion maturation, vacuole formation, and the general appearance of the cytoplasm. HFFs were infected at the time of replating at an MOI of 1 in the presence or absence of 50 μM SMER28. At 96 hpi, cells were fixed with 2% glutaraldehyde and processed for electron microscopy. In contrast to what was observed following treatment with trehalose, the cytoplasm of infected cells treated with SMER28 lacked extensive vacuolation and was comparable to that seen in untreated infected cells (Fig. 11A and B). We observed that there was a large decrease in the amount of virions being enveloped in the cytoplasmic assembly center, but envelopment itself appeared to be successfully taking place based on the few visible virions (Fig. 11G). Also absent in SMER28-treated HFFs were vesicles with membrane whorls and MVBs containing virions with a severely altered morphology. The nuclear capsids appeared comparable, with similar numbers being loaded with DNA in the presence and absence of SMER28 (Fig. 11E and H), as expected from the comparable levels of viral DNA in treated and untreated cells.

HAECs were infected at an MOI of 3 to allow a majority of the cells to be infected and processed for electron microscopy at 96 hpi. The results showed that in HAECs, there was a similar lack of vacuolation in the presence of SMER28 (Fig. 12A and B).

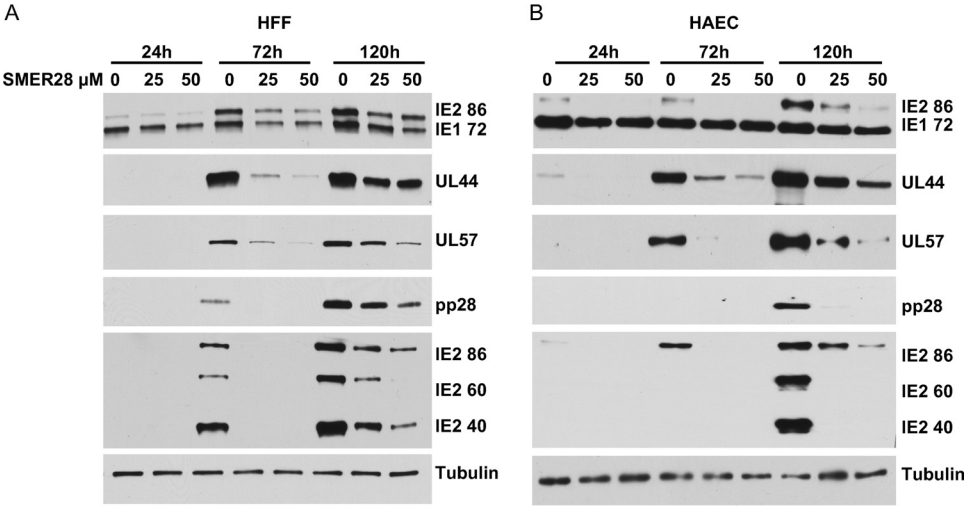

FIG 9 SMER28 reduces levels of early and late viral proteins in HFFs and HAECs. HFFs (A) or HAECs (B) were infected with TB40E at an MOI of 0.5. SMER28 (25 or 50 μM) or DMSO (0) was added to the medium at the time of infection. Cells were harvested at 24, 72, and 120 hpi and processed for Western blotting with antibodies against the IE1 72 and IE2 86 proteins, UL44, UL57, pp28, the late IE2 proteins IE2 60 and IE2 40, and tubulin as a loading control.

However, there was a striking absence of virions in the cytoplasm (Fig. 12G), unlike the treated HFFs, which showed a reduction but not a complete absence of enveloped virions. Extending infection to 120 hpi in SMER28-treated cells yielded a similar lack of cytoplasmic virions in infected HAECs (Fig. 13B and C). The nuclei of SMER28-treated HAECs also contained mostly empty capsids (B capsids) at 96 hpi (Fig. 12H) and at 120 hpi (Fig. 13D), consistent with the reduction in viral genome replication seen in infected HAECs (Fig. 10).

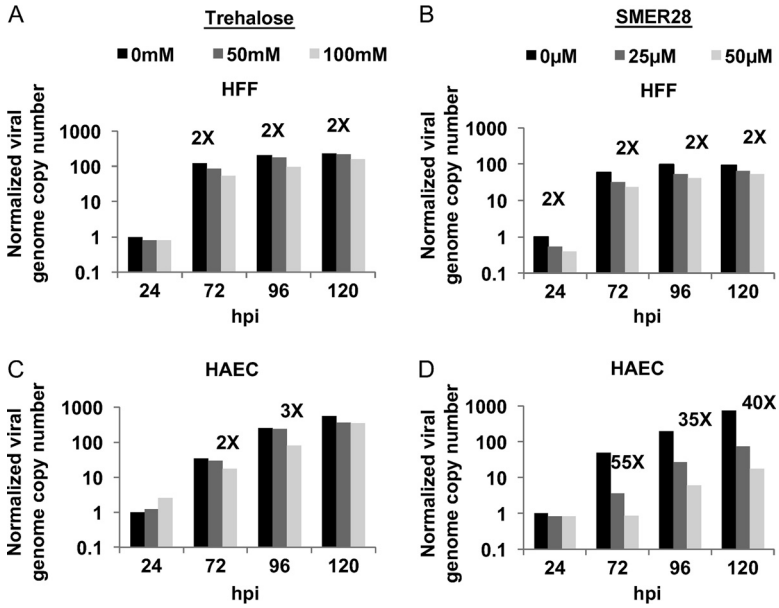

FIG 10 SMER28 but not trehalose has a differential effect on viral DNA synthesis in HFFs and HAECs. HFFs (A and B) or HAECs (C and D) were infected with TB40E at an MOI of 0.5. A total of 50 or 100 mM trehalose (A and C) or 25 or 50 μM SMER28 or DMSO (B and D) was added to the medium at the time of infection. Cell pellets were harvested at the indicated times p.i. DNA was extracted from cells, and viral genome copy numbers relative to cellular GAPDH were determined by quantitative real-time PCR using primers against unspliced UL77 and are displayed as genome copies normalized to values for untreated samples at 24 hpi. Fold changes indicate differences between untreated samples and samples treated with the highest concentration of the drug.

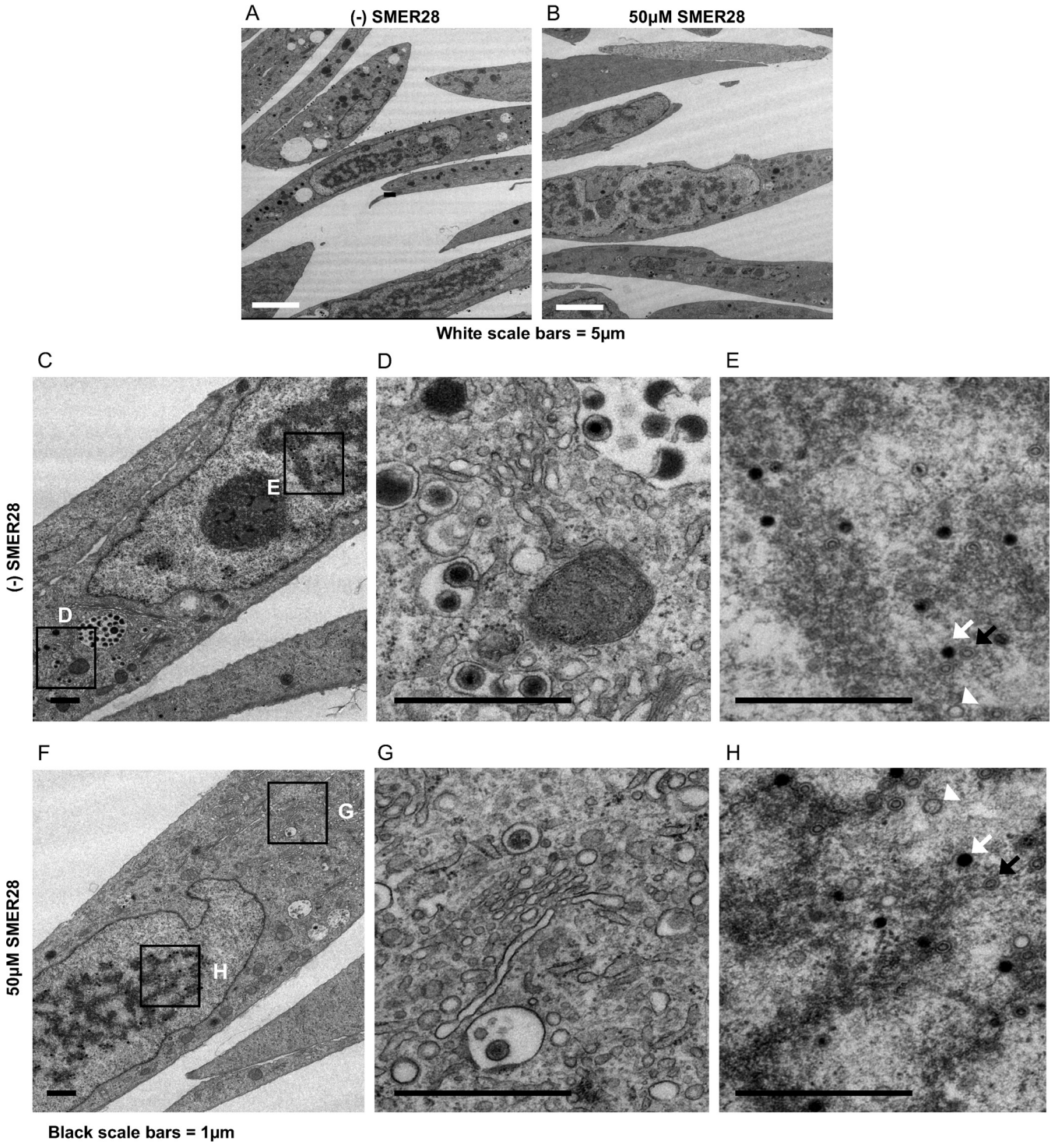

FIG 11 SMER28 does not induce vacuolation of the cytoplasm in infected HFFs. HFFs were infected with TB40E at an MOI of 1 in the presence of DMSO or 50 μM SMER28, as indicated. Cells were fixed with 2% glutaraldehyde and processed for electron microscopy at 96 hpi. Boxes in the left images (C and F) indicate regions of enlargement in the right images (D, E, G, and H). A, B, and C capsids in panels E and H are indicated by white arrowheads, black arrows, and white arrows, respectively.

SMER28 shows differential effects on the levels of the autophagosome marker lipidated LC3B-II in HFFs and HAECs. During autophagy, the native form of cytosolic LC3B (LC3B-I; 18 kDa) is conjugated to phosphatidylethanolamine to form LC3B-II (16 kDa). LC3B-II binds to the membranes of the autophagosome, and following the fusion

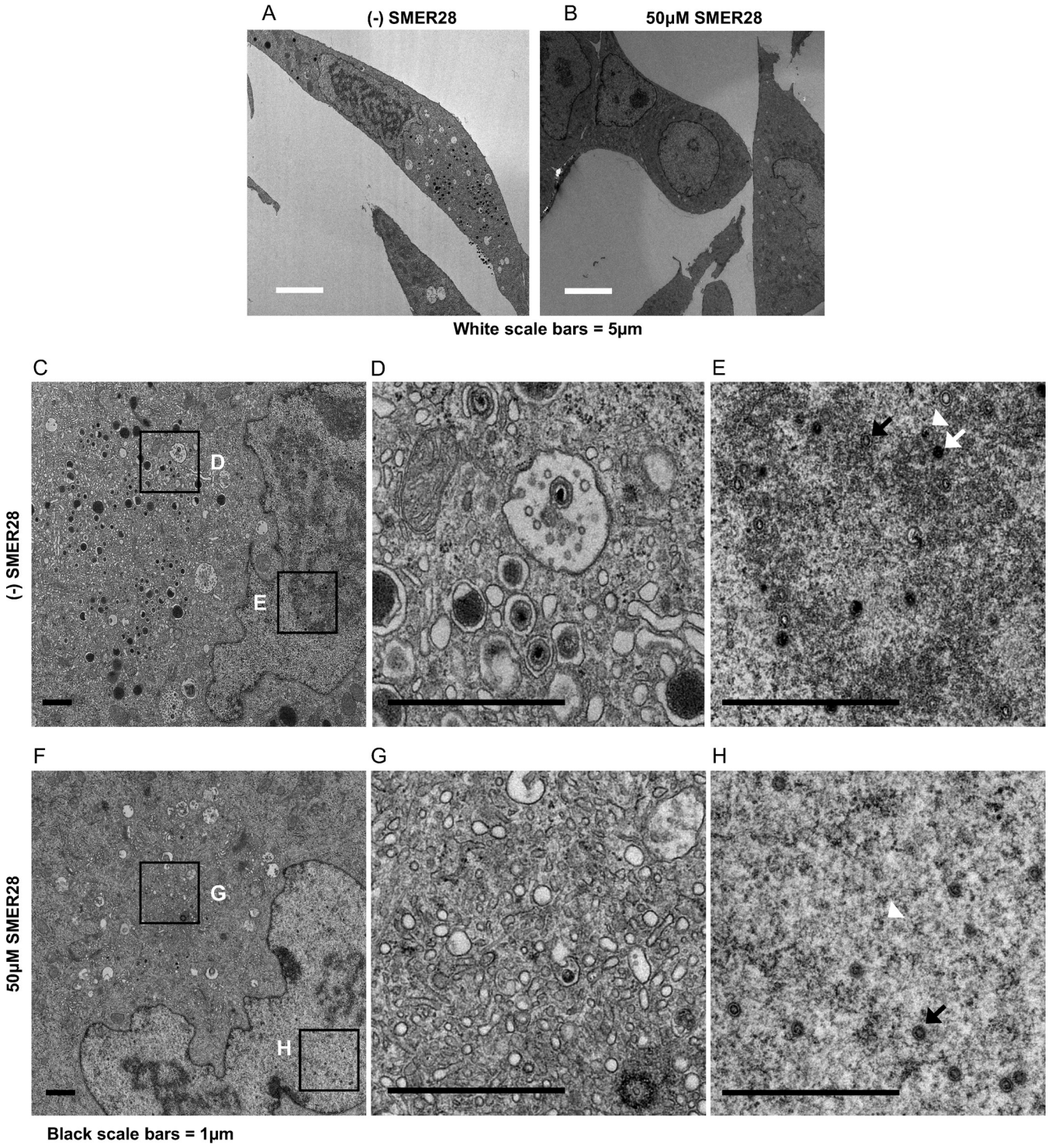

FIG 12 SMER28 treatment blocks production of DNA-filled capsids in the nucleus and mature virions in the cytoplasm and does not induce cytoplasmic vacuolation in HAECs. HAECs were infected with TB40E at an MOI of 3 in the presence of 50 μM SMER28. Cells were fixed with 2% glutaraldehyde and processed for electron microscopy at 96 hpi. Boxes in the left images (C and F) indicate regions of enlargement in the right images (D, E, G, and H). A, B, and C capsids in panels E and H are indicated by white arrowheads, black arrows, and white arrows, respectively.

of the autophagosome with the lysosome, LC3B-II is degraded. One method used to assess the extent of autophagy involves measuring the relative levels of LC3B-I and LCB-II by Western blotting of cell lysates. Our previous studies with trehalose showed that it induced a large increase in the levels of LC3B-II, consistent with the increase in

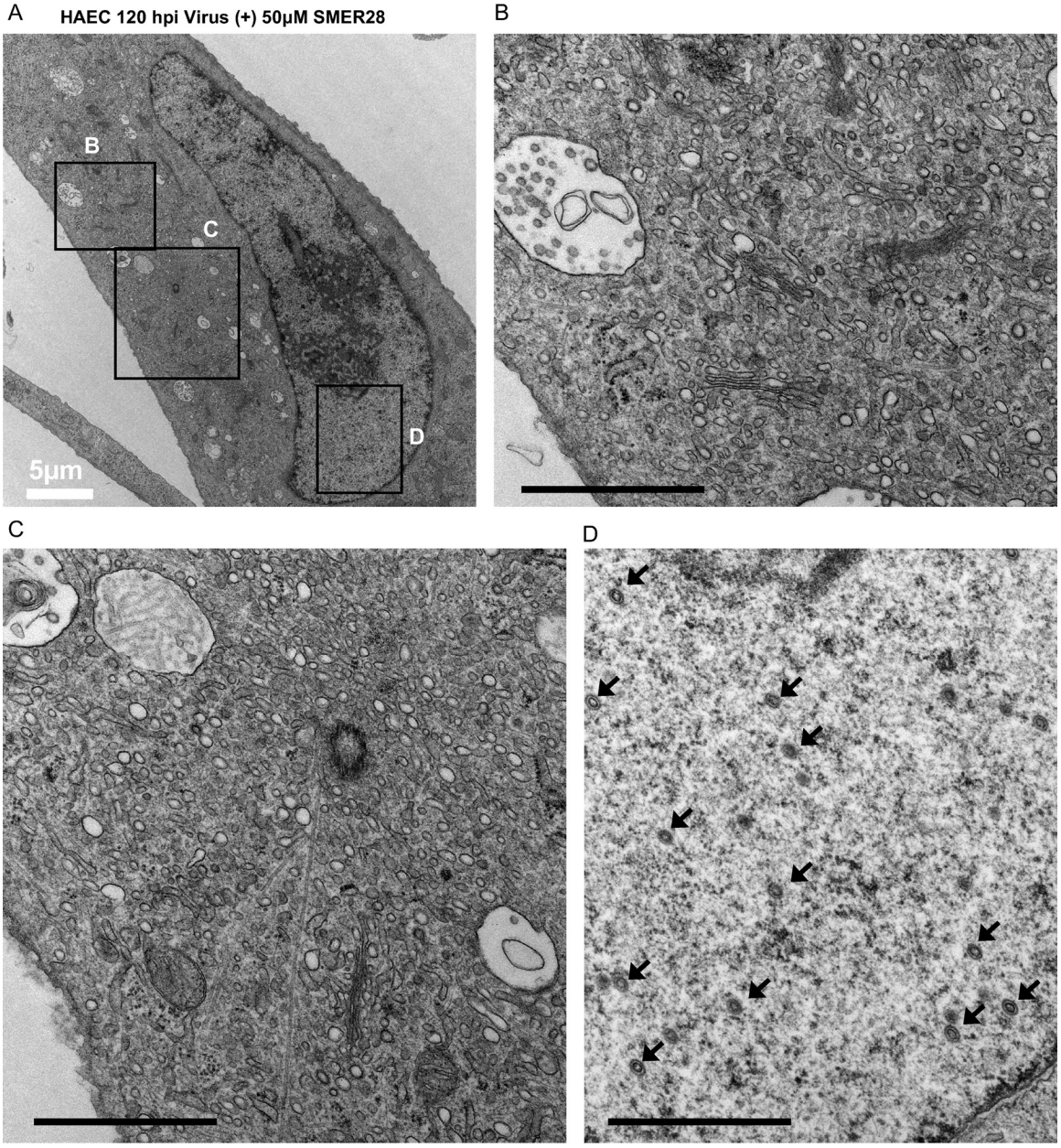

FIG 13 SMER28 treatment blocks production of DNA-filled capsids in the nucleus and mature virions in the cytoplasm and does not induce cytoplasmic vacuolation in HAECs at 120 hpi. HAECs were infected with TB40E at an MOI of 3 in the presence of 50 μM SMER28. Cells were fixed with 2% glutaraldehyde and processed for electron microscopy at 120 hpi. Boxes in the left panels indicate regions of zoom (right panels). Black bars (B to D), 1 μm. Black arrows (D) indicate B capsids.

the number of LC3B-positive (LC3B$^+$) puncta observed in the cytoplasm (1). To determine whether SMER28 has an effect on the levels of LC3B-II comparable to that of trehalose, HFFs (Fig. 14, left) and HAECs (Fig. 14, right) were mock infected or infected at an MOI of 3 with HCMV in the presence or absence of 50 μM SMER28. Cells were harvested, and lysates were prepared for Western blotting at 24 and 72 hpi. SMER28 treatment did not induce substantial changes in the levels of LC3B-II in infected HFFs and caused a slight reduction in LC3B-II levels in uninfected cells at 24 h posttreatment. Uninfected and infected HAECs treated with SMER28 showed a small increase in the levels of LC3B-II at 72 h posttreatment. This moderate effect of SMER28 on the levels of LC3B-II was not due to an increased production of LC3B-II that was accompanied by increased autophagic flux and degradation of the protein, as treatment with bafilomy-

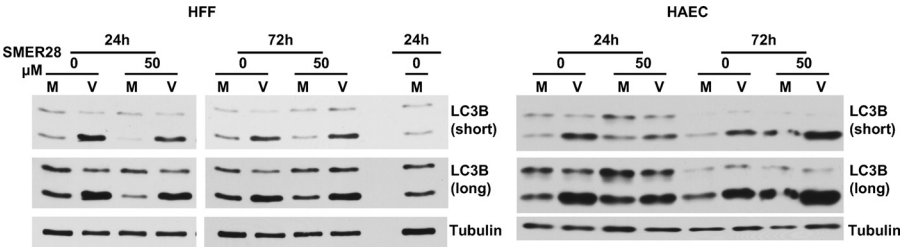

FIG 14 SMER28 treatment modestly increases autophagy in uninfected and infected HAECs but not in HFFs. HFFs or HAECs were mock infected (M) or infected with TB40E at an MOI of 3 (V). A total of 50 μM SMER28 or DMSO was added to the medium at the time of infection. Cells were harvested at 24 and 72 hpi and processed for Western blotting with antibodies against LC3B and tubulin as a loading control. In HFF Western blots, a repeated sample was used to calibrate blotting and exposures between the 2 different gels. Both short and long exposures of LC3B are shown.

cin A1 had similar effects on the accumulation of LC3B-II in SMER28-treated and untreated cells (data not shown). These results appear to be consistent with the those of others who found modest cell type-dependent responses to SMER28 with respect to the accumulation of LC3B-II (20, 22, 24, 27, 28).

Trehalose, but not SMER28, induces acidification of cytoplasmic compartments. Considering the differences in the extents of cellular vacuolation in cells treated with trehalose versus SMER28, we assayed for the acidification of cytoplasmic compartments by staining cells with LysoTracker, a live-cell-permeable fluorescent marker of acidity. We expected trehalose to induce acidification consistent with our previously reported results showing a large trehalose-dependent increase in the number of acidified LC3B-positive compartments (1). For this experiment, HFFs (Fig. 15A) and HAECs (Fig. 15B) were infected at an MOI of 3. Cells were infected in the presence of 50 μM SMER28 or 100 mM trehalose or were untreated. At 96 hpi, cells were stained with LysoTracker for 30 min and fixed. Slips were then counterstained with Hoechst 33342 dye to visualize nuclei and imaged. We observed that there was a clear increase in acidification in both mock-infected and infected cells after treatment with trehalose

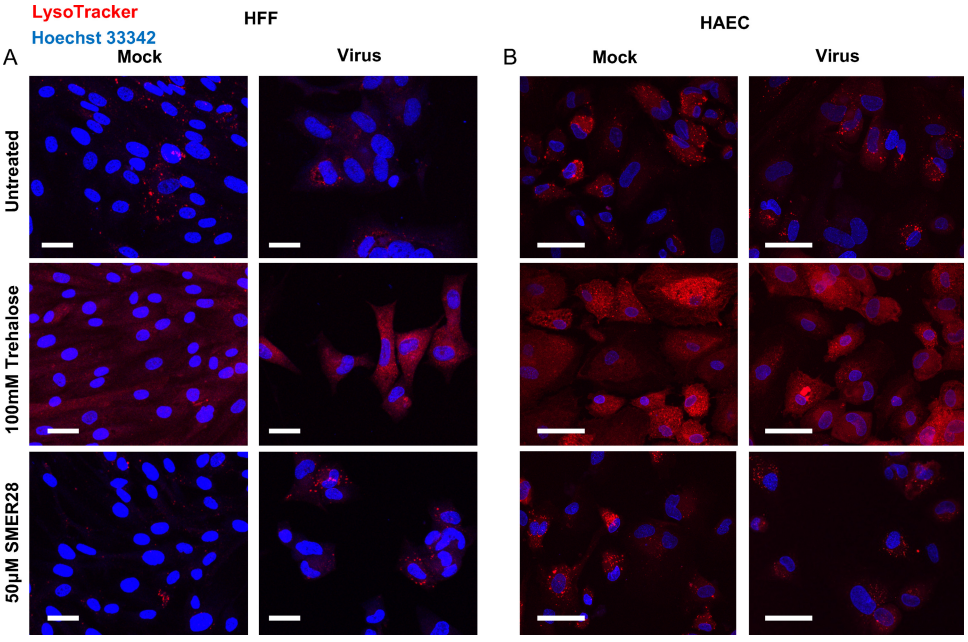

FIG 15 Trehalose, but not SMER28, induces acidification of cytoplasmic compartments. HFFs (A) or HAECs (B) were mock infected or infected with TB40E at an MOI of 3 in the presence of 50 μM SMER28 or 100 mM trehalose or were left untreated and plated onto coverslips at the time of infection. At 96 hpi, cells were stained with LysoTracker and fixed. Nuclei were counterstained with Hoechst 33342 dye. Bars, 50 μm.

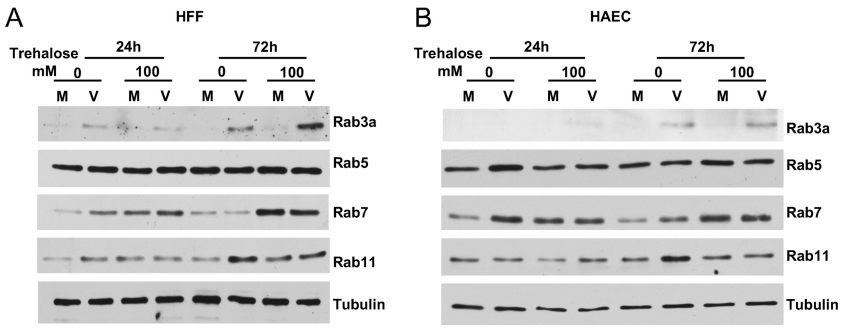

FIG 16 Effect of HCMV infection and trehalose treatment on levels of Rab GTPases. HFFs (A) or HAECs (B) were mock infected (M) or infected with TB40E at an MOI of 3 (V) in the presence or absence of 100 mM trehalose. At 24 and 72 hpi, cells were harvested and processed for Western blotting with antibodies against Rab3a, -5, -7, and -11 and tubulin as a loading control.

but not with SMER28. Acidic puncta in SMER28-treated cells, both mock infected and infected, resembled those of the untreated samples. As a control, we treated the cells with 100 μM chloroquine, an inhibitor of acidification, and found that this compound greatly reduced the intensity of LysoTracker staining in trehalose-treated cells (data not shown).

HCMV infection and trehalose treatment disrupt the levels of Rab GTPases. Based on the above-described results showing the dramatic vacuolation of the cytoplasm and acidification after trehalose treatment in both infected and uninfected cells, we were interested in examining the levels of some key proteins involved in the formation of lysosomes and trafficking between various membrane compartments. The Rab (Ras-like GTPase) family of proteins regulates traffic between membrane compartments (for a review, see reference 29). The >60 identified members of the Rab family in humans perform various regulatory functions in trafficking, and several are involved in regulating autophagy (30, 31). Of the Rabs, Rab7 has gained increasing attention for its importance in lysosome biogenesis and maintenance, the late maturation of autophagosomes and their fusion with lysosomes, and transport from late endosomes to lysosomes (4, 32, 33).

Rab proteins have been shown to have roles in HCMV infection. For example, both the inhibition of Rab6 and the knockdown of Rab27 reduced the production of virus (~4- to 10-fold), and Rab27 was found by EM to be associated with enveloped virions (34, 35). Rab3 was found by EM to colocalize with HCMV gB in subcellular compartments into which enveloped virions had budded (36). An important role for Rab11 was revealed in a study showing that the inhibition of Rab11 by the introduction of dominant negative Rab11 caused a major reduction (~100-fold) in the viral titer (37). We assayed the levels of Rab3a and Rab proteins involved in autophagy and late endosome maturation (Rab5), lysosome biogenesis and fusion of autophagosomes and late endosomes to lysosomes (Rab7), and endosomal recycling to the cell membrane (Rab11). HFFs (Fig. 16A) or HAECs (Fig. 16B) were infected at an MOI of 3 in the presence or absence of 100 mM trehalose. Cell pellets were harvested at 24 and 72 hpi and processed for Western blotting. The results were comparable for HFFs and HAECs. We found that the levels of Rab5 did not change upon infection or treatment with trehalose. In contrast, the levels of Rab3a and Rab11 were higher in untreated infected cells than in uninfected cells at 72 hpi. The level of Rab7 was slightly higher in untreated infected HAECs than in untreated uninfected cells at 24 hpi but not at 72 hpi. These data were consistent with the results of a previously reported proteomic study (62). Notably, treatment with trehalose prevented the increase in Rab11 but not Rab3a levels in infected cells at 72 hpi. The most striking result was the increase in Rab7 levels at 72 hpi in trehalose-treated infected and uninfected cells.

Trehalose, but not SMER28, induces diffuse localization of Rab7 in infected HFFs. In Fig. 16, we show that trehalose treatment caused an increase of Rab7 levels

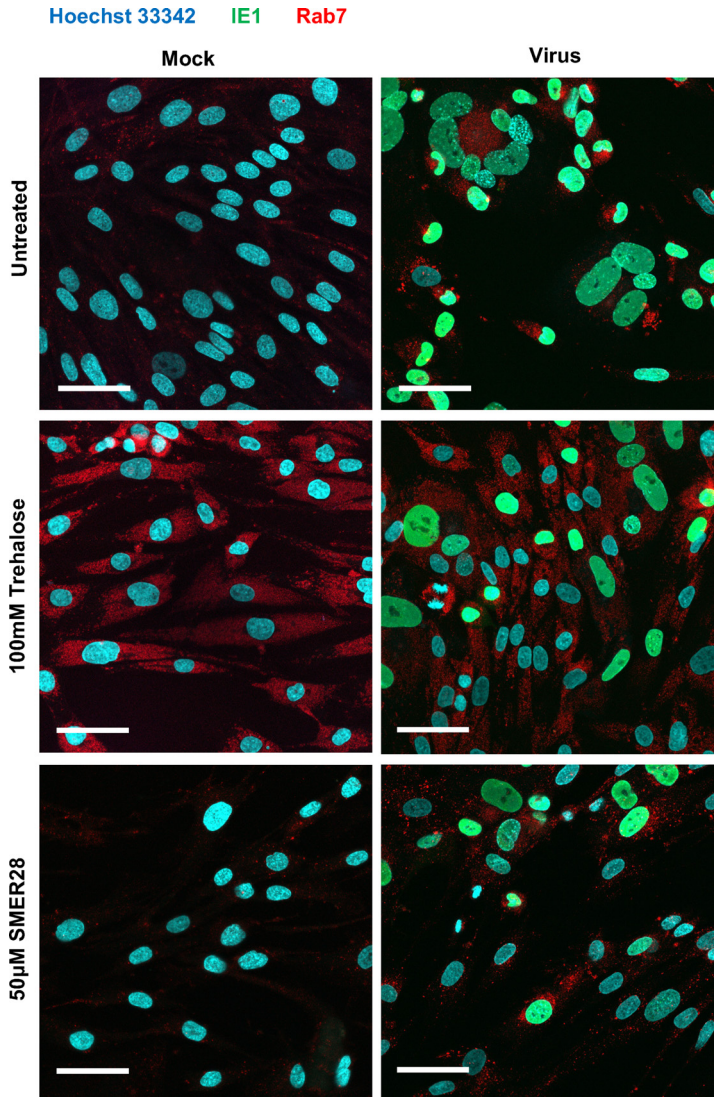

FIG 17 Trehalose, but not SMER28, induces a diffuse localization of Rab7 in infected HFFs. HFFs were mock infected (Mock) or infected with TB40E at an MOI of 0.5 (Virus) in the presence of 50 μM SMER28 or 100 mM trehalose or were left untreated and plated onto coverslips at the time of infection. At 96 hpi, coverslips were fixed and processed for immunofluorescence analysis using antibodies against IE1 72 and Rab7. Nuclei were counterstained with Hoechst 33342 dye. Images of representative cells are shown. Bars, 50 μm.

in both mock-infected and infected HFFs. Rab7 is present on late endosomes as they mature to lysosomes. We examined the cellular localization of Rab7 in untreated, trehalose-treated, and SMER28-treated HFFs during HCMV infection. HFFs were infected at an MOI of 0.5 with 100 mM trehalose or 50 μM SMER28 or left untreated. At 96 hpi, slips were fixed and stained with antibodies against IE1 72 (to show infected cells) and Rab7 and counterstained with Hoechst 33342 dye to visualize nuclei. In both untreated and SMER28-treated cells, Rab7 showed a punctate localization (Fig. 17). In striking contrast, trehalose treatment induced a more diffuse localization of Rab7. Viral assembly centers remained intact, as the localization of the tegument protein pp28 is not altered by trehalose treatment (data not shown), although protein levels are reduced (1).

DISCUSSION

Defects in autophagy have been linked to multiple pathological conditions. It is apparent that autophagy is not a linear process but rather intersects many pathways,

particularly vesicular trafficking. The use of Atg proteins for purposes other than the degradation and recycling of cytosolic components has been shown in multiple contexts, including secretory autophagy, viral exocytosis, intracellular antigen presentation, and extracellular antigen display after phagocytosis (for reviews, see references 38 and 39).

MVBs in particular play key roles in autophagy and vesicular trafficking pathways. Inward budding of the endosomal membranes of the late endosome toward the lumen gives rise to intraluminal vesicles (ILVs) within MVBs. MVBs can be targeted to lysosomes, whereby fusion with the lysosome leads to the degradation of the MVB contents. MVBs can also fuse with autophagosomes to form amphisomes prior to their fusion with the lysosome. Alternatively, MVBs can fuse with the plasma membrane, releasing the contents to the extracellular environment. The ILVs released are often referred to as exosomes, and some appear to contain lipidated LC3 (40).

Multiple viruses utilize components of autophagy and the exosome machinery for the assembly of virions and release of host proteins and RNAs that can affect pathogenesis (for reviews, see references 39 and 41). Notably, RNA viruses use elements of the autophagy pathway not only to facilitate RNA replication but also to acquire an envelope surrounding the capsid and to exit from the cell. For example, picornaviruses may become enclosed within vesicles with autophagy membranes to exit the cell nonlytically and spread to other cells (42). Some flaviviruses also seem to use autophagy membranes and MVBs for cell exit (43–45). In addition, influenza A virus specifically blocks the fusion of autophagosomes with lysosomes (46) and redirects LC3-containing compartments to the plasma membrane to facilitate its budding (47). Although it is believed that herpesviruses undergo secondary envelopment in post-Golgi membrane compartments, the identity of the vesicles that transport the virus to the plasma membrane has not yet been elucidated. However, there is evidence that EBV, KSHV, and VZV use autophagic membranes for their secondary envelopment (6–9). LC3B has been found in purified VZV (6) and EBV (9) particles, and in the case of EBV, the inhibition of autophagic membrane formation via silencing of Atg12 and Atg16 reduced virus output. Taken together, the body of evidence linking autophagy and exocytosis with the life cycle of multiple viruses makes modulation of the autophagy pathway an attractive option in the search for novel strategies to fight viral infections.

Endosomal trafficking, controlled by the Rab proteins, also intersects with the autophagy pathway. Rab11, a protein most commonly associated with plasma membrane-destined recycling endosomes, has been shown to contribute to autophagosome formation and fusion between autophagosomes and recycling endosomes to form amphisomes (30, 48–50). Rab11 is also an essential factor in many viral infections, including herpesvirus infections (37, 51–53). For example, in the case of HCMV, it was shown that the inhibition of Rab11 by the expression of dominant negative Rab11 in the cell significantly inhibited the production of infectious virus (37). In addition, the identification of both Rab11 and LC3B in vesicular compartments containing VZV particles has provided further evidence that there is a convergence of the endosomal and autophagy pathways in the secondary envelopment and egress of some herpesviruses. An elegant study using a live-cell fluorescence microscopy assay also showed that the exocytosis of pseudorabies virus, an alphaherpesvirus, utilizes constitutive secretory mechanisms with vesicles associated with Rab6, -8, and -11 (52, 54).

The expression and function of Rab7, a key protein regulating the fusion of autophagosomes with lysosomes, are disrupted during infection by multiple viruses. For example, hepatitis C virus (HCV) causes the cleavage of the Rab7 adaptor protein RILP, leading to the increased extracellular release of virions (55). Interestingly, the overexpression of the RILP cleavage product was sufficient to induce the observed change in trafficking to one that favors virus release. Another example is EBV, where the fusion of autophagosomes with lysosomes is blocked during lytic infection, and this is associated with reduced Rab7 levels (7).

We initially chose to use trehalose to induce autophagy because it acts independently of the mTOR pathway, which is specifically modified by HCMV for productive

infection. We previously reported that trehalose induced autophagosome formation and autophagic flux in three of its *in vivo* target cells, including HFFs, HAECs, and neural cells derived via the directed differentiation of embryonic stem cells (1). In all of these cell types, trehalose inhibited viral gene expression and the production of cell-free virus. A surprising finding was that there was only a small effect on the levels of cell-associated virus. This suggested that vesicular processes leading to the egress of HCMV might be affected.

The most striking feature of trehalose-treated cells was the massive vacuolation and the presence of membrane whorls throughout the cytoplasm, with many vesicles being in the process of fusing. In addition, there was extensive acidification of cytoplasmic compartments, consistent with our previously reported data showing that the increased numbers of LC3B-positive compartments in trehalose-treated cells were also acidified (1). These results indicate that the vesicles induced by trehalose include late endosomes/MVBs, amphisomes, and lysosomes. When considered with the observation that the MVBs contained a large amount of particulate debris and abnormal virions, we propose that a major effect of trehalose is to direct virus particles to vesicles where they will be degraded. In accord with these results, we show that trehalose treatment of HCMV-infected cells leads to increased Rab7 levels and slightly decreased Rab11 levels, with no effect on Rab5. This trehalose-mediated reciprocal effect on Rab11 and Rab7 likely contributes to the redirection of virions from the pathway leading to release at the plasma membrane to one bound for lysosomal degradation.

After promising results with trehalose, we looked for other mTOR-independent autophagy enhancers to test for anti-HCMV activity, and based on the literature, SMER28 was identified as a good candidate. In general, studies with SMER28 have shown that it has various effects on LC3B, which appear to depend on the cell type. Moreover, the increases in the numbers of LC3B puncta or the levels of LC3B-II have been modest and much smaller than what is observed following treatment with trehalose. For example, one study found increased numbers of LC3B-positive puncta and levels of EGFP–LC3B-II in SMER28-treated HeLa cells (20), while another study showed a slightly reduced endogenous LC3B intensity in SMER28-treated human umbilical vein endothelial cells (HUVECs) along with reduced levels of p62, suggesting increased autophagic flux (27). It was also noted that the there was only a minor change in LC3B-II levels in K562 bone marrow cells treated with SMER28 (24). In the studies reported here, we found that at 50 μM, SMER28 inhibits HCMV infection at least as well as 100 mM trehalose. Based on the lipidation of LC3B to form LC3B-II, there was limited evidence for autophagy induction, and the effect on autophagy appeared to be cell type dependent. SMER28 did not induce a change in the LC3B-II levels in HFFs but increased the LC3B-II levels in both infected and uninfected HAECs at 72 hpi.

As an anti-HCMV compound, SMER28 inhibited the viral life cycle at an earlier point than did trehalose, without the apparent reorganization of the cytoplasmic landscape as observed by electron microscopy and immunofluorescence analysis. In contrast to the effect of trehalose, the cytoplasm of SMER28-treated cells did not show extensive vacuolation or acidification of vesicles for either cell type. In addition, unlike trehalose, SMER28 inhibits viral early proteins and shows reduced amounts of cell-associated virus. The almost complete absence of enveloped virions in both HFFs and HAECs in the presence of SMER28 also suggests that it inhibits HCMV infection upstream of virus secondary envelopment. The effect of SMER28 on viral DNA replication was cell type specific, with infected HAECs showing a much greater sensitivity. This effect is consistent with a much more pronounced defect in the expression of UL57, which is the viral single-stranded DNA binding protein required for viral DNA replication, and a notable absence of viral DNA-containing C capsids in the nucleus.

Taken together, our studies support a model (Fig. 18) in which trehalose both reduces the accumulation of late viral proteins and disturbs the use of trafficking pathways by enveloped HCMV virions in both HFFs and HAECs. Trehalose induces changes in the cytoplasmic landscape and in the Rab family of regulatory proteins, limiting virus release from the cell and potentially redirecting virions to acidified

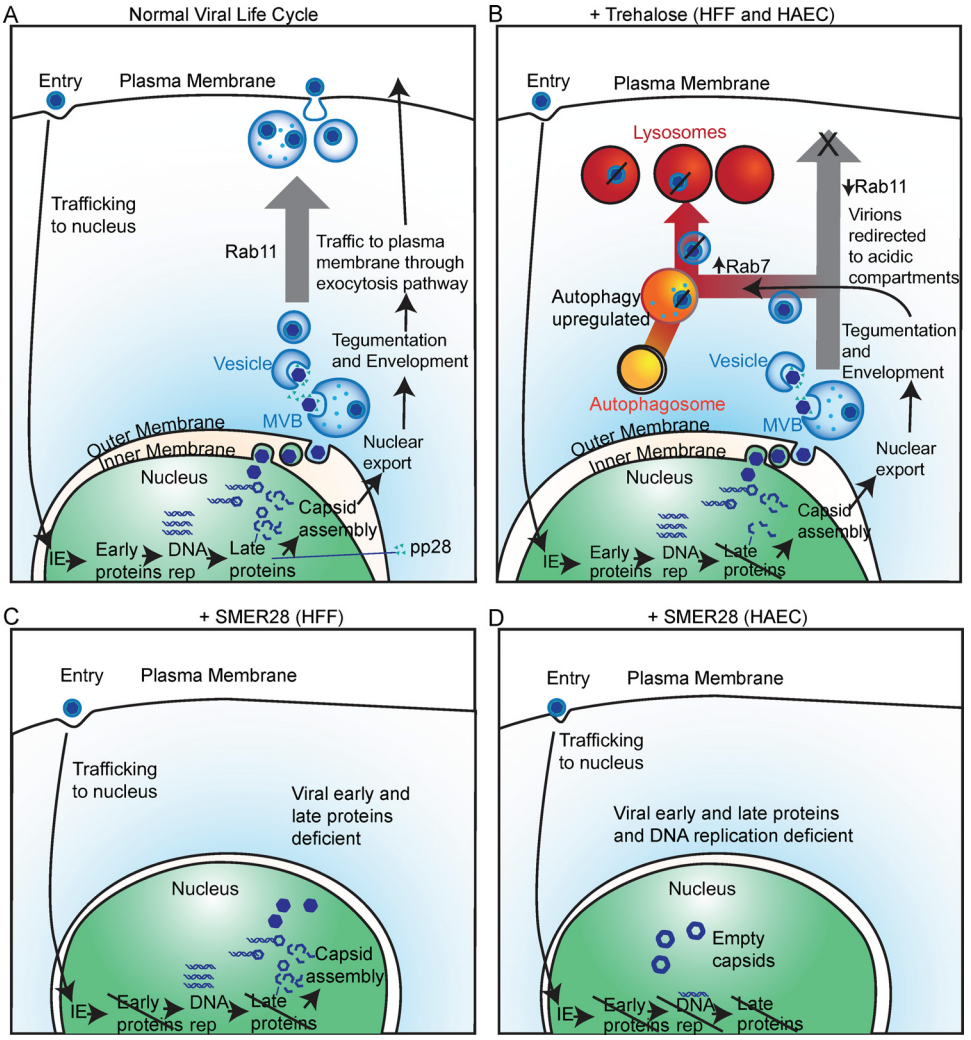

FIG 18 Model for inhibition of HCMV infection by trehalose and SMER28. (A) Diagram of the viral life cycle showing gene expression stages and viral envelopment and egress involving Rab11-dependent trafficking. (B) Trehalose treatment in HFFs and HAECs interferes with the HCMV life cycle by reducing late protein levels and shifting intracellular traffic from the plasma membrane to lysosomes associated with decreased Rab11 and increased Rab7 levels. (C) SMER28 treatment of HFFs blocks expression of early and late proteins, and few enveloped virions are produced. (D) SMER28 treatment of HAECs interferes with early protein expression and viral genome replication, highlighting a cell type specificity in the stage at which HCMV replication is inhibited. DNA rep, DNA replication.

compartments in which they are degraded. In contrast, the antiviral activity of SMER28 appears to be independent of cellular trafficking pathways and interferes with the HCMV life cycle at an earlier point, reducing early protein accumulation in both HFFs and HAECs and delaying viral genome replication in HAECs.

It is important to note that the very large numbers of proteins that are involved in the generation of autophagosomes, the recognition of substrates, the sequestration of the substrates within the vesicles, and the delivery of the cargo to the lysosome, coupled with the redundancy of many of these proteins, provide multiple targets for the activation and inhibition of autophagy. Thus, a comparison of the effects of different "inducers" and "inhibitors" of autophagy on viral infection may give contradictory results, particularly when viral replication may benefit or be impaired from the activation and inhibition of different parts of the autophagy pathway. Likewise, the unknown off-target effects of many of the pharmacological agents being used further complicate the interpretation of data from many experiments. Added to this lack of clarity are the differential effects that may be cell type specific or dependent on the

nutritional state of the cells or the mode of infection (e.g., cell-free virus versus cell-associated virus) (56).

Our studies with trehalose highlight how the cell type may influence conclusions regarding mechanism of autophagy induction. A recent commentary had the title *Mystery Solved*: *Trehalose Kickstarts Autophagy by Blocking Glucose Transport* (19). The studies underlying this commentary specifically showed that trehalose treatment inhibits cellular glucose import through SLC2A (GLUT) transporters in hepatocytes, thus inducing a starvation-like state (18, 57). This leads to the activation of AMP kinase (AMPK) and Unc-51 like autophagy activating kinase 1 (ULK1), the inhibition of mTORC1, and the induction of autophagy. Once in the cytoplasm, trehalose also induced autophagy, and those authors acknowledged that the intracellular actions of trehalose may not be restricted to glucose transport inhibition, the activation of AMPK and ULK1, and the inhibition of mTORC1, particularly in cell types other than hepatocytes (57). We were very interested in those results, as others had previously shown that HCMV-infected cells show an increase in glucose uptake (25) and that blocking GLUT4-mediated glucose transport during infection leads to reduced virus production (26). In contrast, our studies showed that in both uninfected and HCMV-infected primary HFFs and HAECs, trehalose had no negative effect on glucose uptake. It is possible that differences in the GLUT repertoire between HFFs and HAECs and the cell types or overexpression systems used by DeBosch et al. (18) could explain the discrepancies in our results in comparison to theirs. We also observed no evidence for the inhibition of mTORC1 activity in either cell type based on S6K phosphorylation (data not shown). Our results do not negate the potential importance of trehalose treatment for hepatic steatosis through a GLUT-mediated mechanism but show that interpretation of the mechanism must be considered in the context of the specific cells being investigated.

MATERIALS AND METHODS

Cell culture. HFFs were obtained from the American Type Culture Collection and maintained as previously described (58). HAECs were maintained in culture as previously described (58). Culture medium for each cell type was supplemented with trehalose (Sigma-Aldrich) at the concentrations indicated in the figure legends, and medium was filtered. Control medium was filtered in the same manner. Culture medium for each cell type was supplemented with SMER28 (Tocris) prepared in DMSO and added to the medium at the concentrations indicated in the figure legends. An equal volume of DMSO was added to the medium of untreated cells and did not exceed a concentration of 0.05%.

Virus production, titration, and infection. HCMV clinical strain TB40E was maintained in HAECs as previously described (58). The infectious supernatant from HAECs was passaged once in HFFs to obtain higher titers. After centrifugation at 1,000 $\times$ *g* to remove cell debris, virions were pelleted by ultracentrifugation through a sorbitol cushion as described previously (59). Titers of concentrated virus stocks were determined by a plaque assay on HFFs. The MOI was calculated from the PFU counts in HFFs. An equivalent volume of the concentrated supernatant from uninfected cells was used in control mock infections.

HAECs and HFFs were infected with HCMV in the absence or presence of trehalose or SMER28 at the MOIs indicated in the figure legends or mock infected with concentrated tissue culture supernatants. Figures represent data from at least 2 biological replicates. In general, for electron microscopy imaging and for single-cycle growth experiments, an MOI of 0.5 to 1 was used to ensure infection of the majority of HFFs; an MOI of 3 was needed to infect the majority of HAECs, as empirically, we have found that HAECs require a slightly higher input of virus than HFFs to ensure infection of the majority of the cells. When we looked at the effect of trehalose or SMER28 on the production of virion proteins or viral DNA, we used the same amount of input virus (MOI of 0.5). When we assayed cellular proteins or intracellular effects of the drugs on cytoplasmic acidification, we also used the same input of virus and an MOI of 3 for both HFFs and HAECs. To prepare for infection, HFFs were allowed to come to confluence and maintained for 3 days prior to infection to allow exit from the cell cycle. Cells were then trypsinized, infected with HCMV or mock infected, and replated at the time of infection at a lower density to induce synchronous entry into the G_1 phase and progression of the cell cycle. HAECs were infected 24 h after replating. At 6 hpi, virus was removed, cells were washed with phosphate-buffered saline (PBS), and fresh growth medium with or without trehalose or SMER28 was added. In all experiments, culture medium with or without trehalose or SMER28 was replaced every 48 h (corresponding to 48 hpi and 96 hpi).

Glucose uptake assay. The glucose uptake assay was described previously (60). Cells incubated for 4 to 6 h in serum-free medium were washed with Krebs-Ringer-HEPES (KRH) buffer and treated for 15 min with KRH buffer containing 100 mM trehalose, 20 μM cytochalasin B, or 200 nM insulin prior to the addition of radiolabeled [1,2-^{3}H]2-deoxy-D-glucose to a final concentration of 6.5 mM 2DG at 0.5 μCi/well in a 24-well dish. Uptake was halted after 5 min by washing with ice-cold KRH buffer. Cells were lysed by incubation with 0.05 N NaOH. For experiments in which various concentrations of 2DG were assayed (Fig. 7), cells were not serum starved. Cells were washed with KRH buffer and incubated in KRH buffer

with or without 100 mM trehalose prior to the addition of radiolabeled [1,2-^{3}H]2-deoxy-D-glucose at 0.5 μCi/well at the indicated final 2DG concentration. The trehalose incubation time, the 2DG uptake time, and lysis conditions varied, as indicated in the figure legends. Lysates were analyzed in a scintillation counter with a counting duration of 2 min per sample. Counts were normalized to the cell number, which was determined by counting infected and uninfected cells in triplicate wells. Under each condition, three wells were infected and assayed independently.

Statistical analysis. In the glucose uptake assay, error bars indicate standard errors of the means of readings from three wells. Significance was determined by one-way analysis of variance (ANOVA) followed by Dunnett's test. Statistical significance is indicated in the figure legends.

Transmission electron microscopy. Cells were fixed directly in 2% glutaraldehyde–0.1 M cacodylate buffer (pH 7.4) for 15 min at room temperature, followed by incubation at 4°C for at least 4 h. Cell pellets were postfixed in 1% osmium tetroxide in 0.1 M cacodylate buffer for 1 h on ice, stained *en bloc* in 2% uranyl acetate for 1 to 2 h on ice, dehydrated in ethanol on ice, embedded in epoxy resin, sectioned at 60 nm, and collected onto 200-mesh copper grids. Grids were viewed by using a JEOL 1200EX II transmission electron microscope and photographed by using a Gatan digital camera.

Analysis of cell-associated and released viruses. Cell-associated and released viruses were analyzed by a plaque assay on HFFs as described previously (1).

Western blotting. Cells were collected, washed twice with PBS, and resuspended in radioimmunoprecipitation assay (RIPA) lysis and extraction buffer (Pierce) supplemented with 1% sodium dodecyl sulfate (SDS) and 1× Halt protease and phosphatase inhibitor cocktail (Pierce). Lysates were sonicated to shear genomic DNA, and the amount of protein was quantified by a bicinchoninic acid (BCA) protein assay (Thermo Fisher Scientific). Lysates were run on 8%, 10%, or 13% polyacrylamide–SDS gels, transferred onto nitrocellulose membranes, and probed with the following mouse monoclonal antibodies in 5% dry milk in Tris-buffered saline with 0.1% Tween 20 (TBS-T): anti-UL57 (CH167), anti-IE1/IE2 (CH160), anti-UL44, anti-pp28/UL99 (all from Virusys), and anti-IE2 (Chemicon). The following rabbit antibodies in 5% dry milk in TBS-T were used: Rab5 (catalog number 3547; Cell Signaling Technology), Rab7 (catalog number 9367; Cell Signaling Technology), Rab11 (catalog number 2413; Cell Signaling Technology), and Rab3a (EMD Millipore) antibodies. For LC3B, lysates were transferred onto polyvinylidene difluoride (PVDF) membranes as described previously (61) and probed with an antibody to LC3B (Cell Signaling Technology) in 5% bovine serum albumin (BSA) in TBS-T. The LC3B antibody recognizes both native (LC3B-I) and lipid-associated (LC3B-II) forms of LC3B. Mouse anti-α-tubulin (Sigma-Aldrich) was used to control for loading.

Quantitative PCR. DNA was isolated from HAECs and HFFs with the QIAamp DNA blood minikit (Qiagen). To detect viral genomic DNA, qPCR analysis was performed with a CFX96 Touch real-time PCR detection system (Bio-Rad) with 50 ng of DNA per reaction by using TaqMan Universal PCR master mix (Applied Biosystems). Primers and TaqMan dually labeled probes (6-carboxyfluorescein [FAM] [5′] and black hole quencher [3′]) were directed against the GAPDH promoter for cellular DNA and the unspliced UL77 gene for viral DNA. The viral DNA value was normalized to the cellular genomic DNA value. PCR primers and probes were described previously (58).

Immunofluorescence. To determine the acidification of the cytoplasm, cells on coverslips were live stained with 1 mM LysoTracker-red DND-99 dye (Invitrogen) in the presence or absence of trehalose or SMER28 at 37°C. After 30 min, the cells were washed three times with PBS and fixed for 15 min at room temperature with 4% paraformaldehyde in PBS. Nuclei were counterstained with Hoechst 33342 dye (Calbiochem), and coverslips were mounted onto slides with Vectashield mounting medium (Vector Laboratories) for confocal microscopy. Pictures of at least six fields were acquired by using a Leica SP5 confocal microscopy system. For immunostaining, slips were washed three times with PBS and fixed for 15 min at room temperature with 4% paraformaldehyde in PBS. Slips were permeabilized in 0.2% Triton-X in PBS for 5 min, washed twice in PBS, and blocked in 10% normal goat serum (NGS) in PBS for 30 min. Slips were then incubated with primary antibodies against IE1 72 (obtained from B. Britt, University of Alabama, Birmingham) and Rab7 (catalog number 9367; Cell Signaling Technology) diluted in 5% NGS in PBS for 30 min and washed in PBS prior to incubation with Alexa Fluor-conjugated secondary antibodies (Thermo Fisher Scientific) and Hoechst 33342 dye in 5% NGS in PBS for 1 h. Slips were washed with PBS, mounted with Vectashield mounting medium, and imaged on a Leica SP5 confocal microscopy system. Nonspecific rabbit antibody was used as a negative control during staining optimization on infected cells. Images were processed with ImageJ and Adobe Photoshop so that no features were added or deleted.

ACKNOWLEDGMENTS

We appreciate the use of the microscopy resources at UCSD, including the Microscopy Core in the Department of Neurosciences and the Farquhar Electron Microscopy Core in the Department of Cellular and Molecular Medicine. We thank Jennifer Santini for confocal microscopy training and Ying Jones for invaluable help with electron microscopy.

HHS, National Institutes of Health (NIH), provided funding under grant numbers AI113443, AI105882, and HL125028 (to D.H.S.). The National Institute of Neurological Disorders and Stroke (NINDS) provided funding under grant number NS047101 for the Microscopy Core in the Department of Neurosciences.

REFERENCES

1. Belzile JP, Sabalza M, Craig M, Clark E, Morello CS, Spector DH. 2015. Trehalose, an mTOR-independent inducer of autophagy, inhibits human cytomegalovirus infection in multiple cell types. J Virol 90:1259–1277. https://doi.org/10.1128/JVI.02651-15.
2. Bader CA, Shandala T, Ng YS, Johnson IR, Brooks DA. 2015. Atg9 is required for intraluminal vesicles in amphisomes and autolysosomes. Biol Open 4:1345–1355. https://doi.org/10.1242/bio.013979.
3. Tooze SA, Abada A, Elazar Z. 2014. Endocytosis and autophagy: exploitation or cooperation? Cold Spring Harb Perspect Biol 6:a018358. https://doi.org/10.1101/cshperspect.a018358.
4. Guerra F, Bucci C. 2016. Multiple roles of the small GTPase Rab7. Cells 5:E34. https://doi.org/10.3390/cells5030034.
5. Johnson DC, Baines JD. 2011. Herpesviruses remodel host membranes for virus egress. Nat Rev Microbiol 9:382–394. https://doi.org/10.1038/nrmicro2559.
6. Buckingham EM, Jarosinski KW, Jackson W, Carpenter JE, Grose C. 2016. Exocytosis of varicella-zoster virions involves a convergence of endosomal and autophagy pathways. J Virol 90:8673–8685. https://doi.org/10.1128/JVI.00915-16.
7. Granato M, Santarelli R, Farina A, Gonnella R, Lotti LV, Faggioni A, Cirone M. 2014. Epstein-Barr virus blocks the autophagic flux and appropriates the autophagic machinery to enhance viral replication. J Virol 88:12715–12726. https://doi.org/10.1128/JVI.02199-14.
8. Granato M, Santarelli R, Filardi M, Gonnella R, Farina A, Torrisi MR, Faggioni A, Cirone M. 2015. The activation of KSHV lytic cycle blocks autophagy in PEL cells. Autophagy 11:1978–1986. https://doi.org/10.1080/15548627.2015.1091911.
9. Nowag H, Guhl B, Thriene K, Romao S, Ziegler U, Dengjel J, Munz C. 2014. Macroautophagy proteins assist Epstein Barr virus production and get incorporated into the virus particles. EBioMedicine 1:116–125. https://doi.org/10.1016/j.ebiom.2014.11.007.
10. Sanchez V, Greis KD, Sztul E, Britt WJ. 2000. Accumulation of virion tegument and envelope proteins in a stable cytoplasmic compartment during human cytomegalovirus replication: characterization of a potential site of virus assembly. J Virol 74:975–986. https://doi.org/10.1128/JVI.74.2.975-986.2000.
11. Das S, Pellett PE. 2011. Spatial relationships between markers for secretory and endosomal machinery in human cytomegalovirus-infected cells versus those in uninfected cells. J Virol 85:5864–5879. https://doi.org/10.1128/JVI.00155-11.
12. Cepeda V, Esteban M, Fraile-Ramos A. 2010. Human cytomegalovirus final envelopment on membranes containing both trans-Golgi network and endosomal markers. Cell Microbiol 12:386–404. https://doi.org/10.1111/j.1462-5822.2009.01405.x.
13. Das S, Vasanji A, Pellett PE. 2007. Three-dimensional structure of the human cytomegalovirus cytoplasmic virion assembly complex includes a reoriented secretory apparatus. J Virol 81:11861–11869. https://doi.org/10.1128/JVI.01077-07.
14. Mori Y, Koike M, Moriishi E, Kawabata A, Tang H, Oyaizu H, Uchiyama Y, Yamanishi K. 2008. Human herpesvirus-6 induces MVB formation, and virus egress occurs by an exosomal release pathway. Traffic 9:1728–1742. https://doi.org/10.1111/j.1600-0854.2008.00796.x.
15. Fraile-Ramos A, Pelchen-Matthews A, Risco C, Rejas MT, Emery VC, Hassan-Walker AF, Esteban M, Marsh M. 2007. The ESCRT machinery is not required for human cytomegalovirus envelopment. Cell Microbiol 9:2955–2967. https://doi.org/10.1111/j.1462-5822.2007.01024.x.
16. Schauflinger M, Villinger C, Mertens T, Walther P, von Einem J. 2013. Analysis of human cytomegalovirus secondary envelopment by advanced electron microscopy. Cell Microbiol 15:305–314. https://doi.org/10.1111/cmi.12077.
17. Schauflinger M, Villinger C, Walther P. 2013. Three-dimensional visualization of virus-infected cells by serial sectioning: an electron microscopic study using resin embedded cells. Methods Mol Biol 1064:227–237. https://doi.org/10.1007/978-1-62703-601-6_16.
18. DeBosch BJ, Heitmeier MR, Mayer AL, Higgins CB, Crowley JR, Kraft TE, Chi M, Newberry EP, Chen Z, Finck BN, Davidson NO, Yarasheski KE, Hruz PW, Moley KH. 2016. Trehalose inhibits solute carrier 2A (SLC2A) proteins to induce autophagy and prevent hepatic steatosis. Sci Signal 9:ra21. https://doi.org/10.1126/scisignal.aac5472.
19. Mardones P, Rubinsztein DC, Hetz C. 2016. Mystery solved: trehalose kickstarts autophagy by blocking glucose transport. Sci Signal 9:fs2. https://doi.org/10.1126/scisignal.aaf1937.
20. Sarkar S, Perlstein EO, Imarisio S, Pineau S, Cordenier A, Maglathlin RL, Webster JA, Lewis TA, O'Kane CJ, Schreiber SL, Rubinsztein DC. 2007. Small molecules enhance autophagy and reduce toxicity in Huntington's disease models. Nat Chem Biol 3:331–338. https://doi.org/10.1038/nchembio883.
21. Tian Y, Bustos V, Flajolet M, Greengard P. 2011. A small-molecule enhancer of autophagy decreases levels of Abeta and APP-CTF via Atg5-dependent autophagy pathway. FASEB J 25:1934–1942. https://doi.org/10.1096/fj.10-175158.
22. Moy RH, Gold B, Molleston JM, Schad V, Yanger K, Salzano MV, Yagi Y, Fitzgerald KA, Stanger BZ, Soldan SS, Cherry S. 2014. Antiviral autophagy restricts Rift Valley fever virus infection and is conserved from flies to mammals. Immunity 40:51–65. https://doi.org/10.1016/j.immuni.2013.10.020.
23. Ma T, Li J, Xu Y, Yu C, Xu T, Wang H, Liu K, Cao N, Nie BM, Zhu SY, Xu S, Li K, Wei WG, Wu Y, Guan KL, Ding S. 2015. Atg5-independent autophagy regulates mitochondrial clearance and is essential for iPSC reprogramming. Nat Cell Biol 17:1379–1387. https://doi.org/10.1038/ncb3256.
24. Doulatov S, Vo LT, Macari ER, Wahlster L, Kinney MA, Taylor AM, Barragan J, Gupta M, McGrath K, Lee HY, Humphries JM, DeVine A, Narla A, Alter BP, Beggs AH, Agarwal S, Ebert BL, Gazda HT, Lodish HF, Sieff CA, Schlaeger TM, Zon LI, Daley GQ. 2017. Drug discovery for Diamond-Blackfan anemia using reprogrammed hematopoietic progenitors. Sci Transl Med 9:eaah5645. https://doi.org/10.1126/scitranslmed.aah5645.
25. Landini MP. 1984. Early enhanced glucose uptake in human cytomegalovirus-infected cells. J Gen Virol 65(Part 7):1229–1232. https://doi.org/10.1099/0022-1317-65-7-1229.
26. Yu Y, Maguire TG, Alwine JC. 2011. Human cytomegalovirus activates glucose transporter 4 expression to increase glucose uptake during infection. J Virol 85:1573–1580. https://doi.org/10.1128/JVI.01967-10.
27. Kalamida D, Karagounis IV, Giatromanolaki A, Koukourakis MI. 2014. Important role of autophagy in endothelial cell response to ionizing radiation. PLoS One 9:e102408. https://doi.org/10.1371/journal.pone.0102408.
28. Shen D, Coleman J, Chan E, Nicholson TP, Dai L, Sheppard PW, Patton WF. 2011. Novel cell- and tissue-based assays for detecting misfolded and aggregated protein accumulation within aggresomes and inclusion bodies. Cell Biochem Biophys 60:173–185. https://doi.org/10.1007/s12013-010-9138-4.
29. Stenmark H. 2009. Rab GTPases as coordinators of vesicle traffic. Nat Rev Mol Cell Biol 10:513–525. https://doi.org/10.1038/nrm2728.
30. Szatmari Z, Sass M. 2014. The autophagic roles of Rab small GTPases and their upstream regulators: a review. Autophagy 10:1154–1166. https://doi.org/10.4161/auto.29395.
31. Ao X, Zou L, Wu Y. 2014. Regulation of autophagy by the Rab GTPase network. Cell Death Differ 21:348–358. https://doi.org/10.1038/cdd.2013.187.
32. Wen H, Zhan L, Chen S, Long L, Xu E. 10 February 2017. Rab7 may be a novel therapeutic target for neurologic diseases as a key regulator in autophagy. J Neurosci Res https://doi.org/10.1002/jnr.24034.
33. Hyttinen JM, Niittykoski M, Salminen A, Kaarniranta K. 2013. Maturation of autophagosomes and endosomes: a key role for Rab7. Biochim Biophys Acta 1833:503–510. https://doi.org/10.1016/j.bbamcr.2012.11.018.
34. Fraile-Ramos A, Cepeda V, Elstak E, van der Sluijs P. 2010. Rab27a is required for human cytomegalovirus assembly. PLoS One 5:e15318. https://doi.org/10.1371/journal.pone.0015318.
35. Indran SV, Britt WJ. 2011. A role for the small GTPase Rab6 in assembly of human cytomegalovirus. J Virol 85:5213–5219. https://doi.org/10.1128/JVI.02605-10.
36. Homman-Loudiyi M, Hultenby K, Britt W, Soderberg-Naucler C. 2003. Envelopment of human cytomegalovirus occurs by budding into Golgi-derived vacuole compartments positive for gB, Rab 3, trans-Golgi network 46, and mannosidase II. J Virol 77:3191–3203. https://doi.org/10.1128/JVI.77.5.3191-3203.2003.
37. Krzyzaniak MA, Mach M, Britt WJ. 2009. HCMV-encoded glycoprotein M (UL100) interacts with Rab11 effector protein FIP4. Traffic 10:1439–1457. https://doi.org/10.1111/j.1600-0854.2009.00967.x.
38. Munz C. 2016. Autophagy proteins in antigen processing for presenta-

tion on MHC molecules. Immunol Rev 272:17–27. https://doi.org/10.1111/imr.12422.
39. Münz C. 2017. The autophagic machinery in viral exocytosis. Front Microbiol 8:269. https://doi.org/10.3389/fmicb.2017.00269.
40. Pallet N, Sirois I, Bell C, Hanafi LA, Hamelin K, Dieude M, Rondeau C, Thibault P, Desjardins M, Hebert MJ. 2013. A comprehensive characterization of membrane vesicles released by autophagic human endothelial cells. Proteomics 13:1108–1120. https://doi.org/10.1002/pmic.201200531.
41. Sadeghipour S, Mathias RA. 2017. Herpesviruses hijack host exosomes for viral pathogenesis. Semin Cell Dev Biol 67:91–100. https://doi.org/10.1016/j.semcdb.2017.03.005.
42. Bird SW, Maynard ND, Covert MW, Kirkegaard K. 2014. Nonlytic viral spread enhanced by autophagy components. Proc Natl Acad Sci U S A 111:13081–13086. https://doi.org/10.1073/pnas.1401437111.
43. Ren H, Elgner F, Jiang B, Himmelsbach K, Medvedev R, Ploen D, Hildt E. 2016. The autophagosomal SNARE protein syntaxin 17 is an essential factor for the hepatitis C virus life cycle. J Virol 90:5989–6000. https://doi.org/10.1128/JVI.00551-16.
44. Shrivastava S, Devhare P, Sujijantarat N, Steele R, Kwon YC, Ray R, Ray RB. 2015. Knockdown of autophagy inhibits infectious hepatitis C virus release by the exosomal pathway. J Virol 90:1387–1396. https://doi.org/10.1128/JVI.02383-15.
45. Wu YW, Mettling C, Wu SR, Yu CY, Perng GC, Lin YS, Lin YL. 2016. Autophagy-associated dengue vesicles promote viral transmission avoiding antibody neutralization. Sci Rep 6:32243. https://doi.org/10.1038/srep32243.
46. Gannage M, Dormann D, Albrecht R, Dengjel J, Torossi T, Ramer PC, Lee M, Strowig T, Arrey F, Conenello G, Pypaert M, Andersen J, Garcia-Sastre A, Munz C. 2009. Matrix protein 2 of influenza A virus blocks autophagosome fusion with lysosomes. Cell Host Microbe 6:367–380. https://doi.org/10.1016/j.chom.2009.09.005.
47. Beale R, Wise H, Stuart A, Ravenhill BJ, Digard P, Randow F. 2014. A LC3-interacting motif in the influenza A virus M2 protein is required to subvert autophagy and maintain virion stability. Cell Host Microbe 15:239–247. https://doi.org/10.1016/j.chom.2014.01.006.
48. Longatti A, Lamb CA, Razi M, Yoshimura S, Barr FA, Tooze SA. 2012. TBC1D14 regulates autophagosome formation via Rab11- and ULK1-positive recycling endosomes. J Cell Biol 197:659–675. https://doi.org/10.1083/jcb.201111079.
49. Longatti A, Tooze SA. 2012. Recycling endosomes contribute to autophagosome formation. Autophagy 8:1682–1683. https://doi.org/10.4161/auto.21486.
50. Szatmari Z, Kis V, Lippai M, Hegedus K, Farago T, Lorincz P, Tanaka T, Juhasz G, Sass M. 2014. Rab11 facilitates cross-talk between autophagy and endosomal pathway through regulation of Hook localization. Mol Biol Cell 25:522–531. https://doi.org/10.1091/mbc.E13-10-0574.
51. Vale-Costa S, Amorim MJ. 2016. Recycling endosomes and viral infection. Viruses 8:64. https://doi.org/10.3390/v8030064.
52. Hogue IB, Scherer J, Enquist LW. 2016. Exocytosis of alphaherpesvirus virions, light particles, and glycoproteins uses constitutive secretory mechanisms. mBio 7:e00820-16. https://doi.org/10.1128/mBio.00820-16.
53. Hollinshead M, Johns HL, Sayers CL, Gonzalez-Lopez C, Smith GL, Elliott G. 2012. Endocytic tubules regulated by Rab GTPases 5 and 11 are used for envelopment of herpes simplex virus. EMBO J 31:4204–4220. https://doi.org/10.1038/emboj.2012.262.
54. Hogue IB, Bosse JB, Hu JR, Thiberge SY, Enquist LW. 2014. Cellular mechanisms of alpha herpesvirus egress: live cell fluorescence microscopy of pseudorabies virus exocytosis. PLoS Pathog 10:e1004535. https://doi.org/10.1371/journal.ppat.1004535.
55. Wozniak AL, Long A, Jones-Jamtgaard KN, Weinman SA. 2016. Hepatitis C virus promotes virion secretion through cleavage of the Rab7 adaptor protein RILP. Proc Natl Acad Sci U S A 113:12484–12489. https://doi.org/10.1073/pnas.1607277113.
56. Meier JL, Grose C. 2017. Variable effects of autophagy induction by trehalose on herpesviruses depending on conditions of infection. Yale J Biol Med 90:25–33.
57. Mayer AL, Higgins CB, Heitmeier MR, Kraf TE, Qian T, Crowley JR, Hyrc K, Beatty WL, Yarasheski KE, Hruz PW, DeBosch BJ. 2016. SLC2A8 (GLUT8) is a mammalian trehalose transporter required for trehalose-induced autophagy. Sci Rep 6:38586. https://doi.org/10.1038/srep38586.
58. DuRose JB, Li J, Chien S, Spector DH. 2012. Infection of vascular endothelial cells with human cytomegalovirus under fluid shear stress reveals preferential entry and spread of virus in flow conditions simulating atheroprone regions of the artery. J Virol 86:13745–13755. https://doi.org/10.1128/JVI.02244-12.
59. Belzile JP, Stark TJ, Yeo GW, Spector DH. 2015. Human cytomegalovirus infection of human embryonic stem cell-derived primitive neural stem cells is restricted at several steps but leads to the persistence of viral DNA. J Virol 88:4021–4039. https://doi.org/10.1128/JVI.03492-13.
60. Yamamoto N, Ueda-Wakagi M, Sato T, Kawasaki K, Sawada K, Kawabata K, Akagawa M, Ashida H. 2015. Measurement of glucose uptake in cultured cells. Curr Protoc Pharmacol 71:12.14.1–12.14.26. https://doi.org/10.1002/0471141755.ph1214s71.
61. Klionsky DJ, Abdalla FC, Abeliovich H, Abraham RT, Acevedo-Arozena A, Adeli K, Agholme L, Agnello M, Agostinis P, Aguirre-Ghiso JA, Ahn HJ, Ait-Mohamed O, Ait-Si-Ali S, Akematsu T, Akira S, Al-Younes HM, Al-Zeer MA, Albert ML, Albin RL, Alegre-Abarrategui J, Aleo MF, Alirezaei M, Almasan A, Almonte-Becerril M, Amano A, Amaravadi R, Amarnath S, Amer AO, Andrieu-Abadie N, Anantharam V, Ann DK, Anoopkumar-Dukie S, Aoki H, Apostolova N, Arancia G, Aris JP, Asanuma K, Asare NY, Ashida H, Askanas V, Askew DS, Auberger P, Baba M, Backues SK, Baehrecke EH, Bahr BA, Bai XY, Bailly Y, Baiocchi R, Baldini G, et al. 2012. Guidelines for the use and interpretation of assays for monitoring autophagy. Autophagy 8:445–544. https://doi.org/10.4161/auto.19496.
62. Weekes MP, Tomasec P, Huttlin EL, Fielding CA, Nusinow D, Stanton RJ, Wang EC, Aicheler R, Murrell I, Wilkinson GW, Lehner PJ, Gygi SP. 2014. Quantitative temporal viromics: an approach to investigate host-pathogen interaction. Cell 157:1460–1472. https://doi.org/10.1016/j.cell.2014.04.028.